Technical Report Documentation Page

1. Report No. PSU-2010-07	2. Government Accession No.	3. Recipient's Catalog No.
4. Title and Subtitle Utilizing Coal Fly Ash and Recycled Glass in Developing Green Concrete Materials		**5. Report Date** June 2012
		6. Performing Organization Code
7. Author(s) Farshad Rajabipour, Seyed (Afshin) Shafaatian, Jared Wright		**8. Performing Organization Report** LTI 2012-03
9. Performing Organization Name and Address The Thomas D. Larson Pennsylvania Transportation Institute The Pennsylvania State University 201 Transportation Research Building University Park, PA, 16802-4710		**10. Work Unit No. (TRAIS)**
		11. Contract or Grant No. DTRT07-G-0003
12. Sponsoring Agency Name and Address U.S. Department of Transportation Research and Innovative Technology Administration UTC Program, RDT-30 1200 New Jersey Ave., SE Washington, DC 20590		**13. Type of Report and Period Covered** Final Report 6/1/2010-8/31/2011
		14. Sponsoring Agency Code
15. Supplementary Notes		

16. Abstract

The environmental impact of Portland cement concrete production has motivated researchers and the construction industry to evaluate alternative technologies for incorporating recycled cementing materials and recycled aggregates in concrete. One such technology is based on using pulverized glass as sand or pozzolan. Currently in the United States more than 600,000 tons/year of recycled glass bottles are stockpiled due to prohibitive shipping costs from recycling locations to glass melting factories. This project demonstrates the potential use of this waste material along with fly ash (another industrial byproduct with landfill rate of 42.4 million tons/year) in developing durable and environmentally positive concretes that can be used for various transportation applications. Toward this objective, the project included two main tasks. In the first task, the deleterious alkali-silica reaction (ASR) induced by the use of silicate glass aggregates was mitigated via the use of fly ash. Mixtures were prepared using one of six different fly ashes. The main objective of this task was to better understand the mechanisms by which fly ash mitigates ASR and to identify factors that most significantly determine fly ash effectiveness against ASR. Through a combination of advanced analytical measurements and numerical simulations, it can be concluded that fly ash is effective against ASR by (a) reducing the alkalinity of pore solution by alkali binding, (b) reducing the mass transport in concrete, (c) improving the tensile strength of concrete, and (d) reducing the aggregate dissolution rate by reducing the concentration of OH^- ions per unit surface area of siliceous aggregates. In addition, fly ashes with low Cao and alkali content and high SiO_2 and Al_2O_3 contents were found to be most effective against ASR. The goal of the second task was to provide recommendations and design tools for engineers and materials suppliers to allow proper proportioning and production of "Glasscrete" mixtures (i.e., concrete containing recycled glass fine aggregates as 100% replacement of natural sand. Several Glasscrete mixtures with target slump, air content, and compressive strength were prepared and their fresh and hardened properties compared against concretes with natural sand. All mixtures contained 20% class F fly ash as mass replacement of Portland cement to mitigate ASR. It was found that the use of glass sand results in a reduction in the compressive strength of concrete, potentially due to weakening of the aggregate-paste bonding. In comparison with natural sand concrete, Glasscrete was found to have better workability, lower water sorptivity, lower chloride permeability, and lower coefficient of thermal expansion. On the other hand, Glasscrete showed lower resistance against abrasion.

17. Key Words Portland cement concrete, glasscrete, pozzolan, fly ash, recycled materials, glass aggregates, alkali-silica, water sorptivity, chloride permeability, thermal expansion		18. Distribution Statement	
19. Security Classif. (of this report) Unclassified	**20. Security Classif. (of this page)** Unclassified	**21. No. of Pages** 51	**22. Price**

Form DOT F 1700.7   **(8-72)**   **Reproduction of Complete Page Authorized**

EXECUTIVE SUMMARY

The environmental impact of Portland cement concrete production has motivated researchers and the construction industry to evaluate alternative technologies for incorporating recycled cementing materials and recycled aggregates in concrete. One such technology is based on using pulverized glass as sand or pozzolan. Currently in the United States more than 600,000 tons/year of recycled glass bottles are stockpiled due to prohibitive shipping costs from recycling locations to glass melting factories. This project demonstrates the potential use of this waste material along with fly ash (another industrial byproduct with landfill rate of 42.4 million tons/year) in developing durable and environmentally positive concretes that can be used for various transportation applications.

Toward this objective, the project included two main tasks. In the first task, the deleterious alkali-silica reaction (ASR) induced by the use of silicate glass aggregates was mitigated via the use of fly ash. Mixtures were prepared by using one of the six different fly ashes (four class F and two class C ashes per ASTM C618); and the fly ash dosage to safely control ASR was determined according to the ASTM C1567 test. The main objective of this task was to better understand the mechanisms by which fly ash mitigates ASR, and to identify factors that most significantly determine fly ash effectiveness against ASR. Through a combination of advanced analytical measurements and numerical simulations, it can be concluded that fly ash is effective against ASR by (a) reducing the alkalinity of pore solution through alkali binding, (b) reducing the mass transport in concrete, (c) improving the tensile strength of concrete, and (d) reducing the aggregate dissolution rate by reducing the concentration of OH^- ions per unit surface area of siliceous aggregates. In addition, fly ashes with low Cao and alkali content and high SiO_2 and Al_2O_3 contents were found to be most effective against ASR.

The goal of the second task of this project was to provide recommendations and design tools for engineers and materials suppliers to allow proper proportioning and production of "Glasscrete" mixtures (i.e., concrete containing recycled glass fine aggregates as 100% replacement of natural sand). In this task, Glasscrete mixtures with target slump, air content, and compressive strength were prepared and their fresh and hardened properties were compared against concretes with natural sand. Specifically, three Glasscrete mixtures were prepared, including a 5,000-psi, 5-inch slump concrete for building superstructures, a 4,000-psi, 5-inch slump concrete for bridge decks, and a 4,000-psi, 1.5-inch slump concrete for slip-form pavements. All mixtures contained 20% class F fly ash as mass replacement of Portland cement to mitigate ASR. It was found that the use of glass sand resulted in a reduction in the compressive strength of concrete, potentially due to weakening of the aggregate-paste bonding. The relationship between w/cm and 7-day and 28-day compressive strengths was established to allow proper proportioning of Glasscrete mixtures. In comparison with natural sand concrete, Glasscrete was found to have a better workability, lower water sorptivity, lower chloride permeability, and lower coefficient of thermal expansion. On the other hand, Glasscrete showed lower resistance against abrasion.

CHAPTER 1:
INTRODUCTION AND PROJECT OBJECTIVES

1.1.   Introduction

Portland cement concrete is the most widely used material in construction of the transportation and energy infrastructure. Since development of Ordinary Portland Cement (OPC) around the turn of the 19th Century, industry and academia have teamed together in the search for ways to make concrete stronger, more durable, and more economical (Mindess et al. 2003). Design standards and specifications (e.g., ACI 318 Building Code; ACI 211; PCA Design Manual; ASTM and AASHTO specifications) have been created and expert committees have been formed to achieve these objectives. Concrete, when designed and constructed properly, is a versatile, economical, and durable material. In 2011, 430 million tons of ready-mixed concrete was produced in the United States, which corresponds to a per capita consumption of approximately 1.43 tons per person per year (PCA 2011). In the same year, Portland cement production in the world has reached 3,400 million tons (approximately 485 kg per capita) (USGS 2012). The energy- and carbon-intensity of cement production (embodied energy ≈ 5.3 MJ/kg; CO_2 footprint ≈ 0.97 kg/kg) (Hanle et al. 2012) has been a subject of emphasis recently to make concrete a more environmentally-friendly product. Greener concretes can be produced by incorporating recycled or industrial waste materials instead of the virgin aggregates and Portland cement. One such technology that was explored in this project is based on utilizing post-consumer glass cullet (i.e., crushed bottle glass) as fine aggregates in concrete along with the use of fly ash (a byproduct of coal-based electricity production) as partial Portland cement replacement.

Information gathered by the United States Environmental Protection Agency (USEPA) in 2010 states that only 27.1% (3.13 million tons) of the 11.53 million tons of post-consumer glass (i.e., glass bottles and window plates) generated annually in the United States is currently recycled (Municipal 2011). The remaining 72.9% of post-consumer glass is discarded along with other household wastes into landfills. Of the 3.13 million tons of glass collected for recycling, 80% is recycled into new glass (Reindl 2003). The other 20% (approximately 600,000 tons/year) is subsequently stockpiled (Figure 1.1) or sent back to landfills. The main reason behind imperfect recycling of the collected glass is the transportation costs associated with shipping glass from collection points to glass melting facilities. This problem is specifically acute in densely populated areas (e.g., Northeastern States) as well as remote areas (e.g., Hawaii and Rocky Mountain States). Other factors contributing to lowering the recycling rate of glass includes mixed glass colors in waste streams and deleterious organics (Reindl 2003). This research is focused on developing durable concrete materials that can allow incorporation of those 600,000 tons/yr of glass cullet as fine aggregates into concrete. Such concrete mixtures will be termed "Glasscrete" in this report.

Figure 1-1: Glass cullet stockpile in West Virginia (1993)

1.2. Objectives and Scope

Green concrete materials produced based on outcomes of this research can be used in various transportation-related applications such as highway barriers, pavements, piers, platforms, and buildings. The main challenge in producing durable glass-based concretes is the deleterious alkali-silica reaction (ASR) between glass particles and the cement paste matrix (Rajabipour et al. 2010). The amorphous silicate structure of glass is attacked by hydroxyl (OH^-) ions in concrete's pore solution. As such, glass aggregates gradually dissolve and are converted to a highly hygroscopic silica gel that absorbs water, swells, and cracks concrete. Figure 1-2 shows typical damage induced by ASR in concrete.

Figure 1-2: ASR crack manifestation (Folliard et al. 2006)

In this project, fly ash was used to mitigate potential ASR deteriorations that could otherwise occur due to use of siliceous glass aggregates. Prior research on natural siliceous aggregates (e.g., opal) has shown that ASTM C618 fly ash can be effective in controlling ASR expansions (Thomas 2011); however, it is not clear how fly ash mitigates ASR. To optimize the use of fly ash and minimize the potential negative impacts on concrete's early-age strength, it is important to determine exactly how fly ash prevents ASR and what ash properties (e.g., composition, fineness, glass content) determine its effectiveness. Furthermore, it is important to evaluate the properties of concrete containing glass fine aggregates and fly ash to ensure that such concretes can be produced with desired strength, workability, and durability.

As such, this project was aimed at two major technical objectives:
1- Understanding the mechanism by which fly ash mitigates ASR, and identifying factors that most significantly determine fly ash effectiveness against ASR; and
2- Preparation and evaluation of concrete mixture that includes glass fine aggregates and fly ash to ensure desirable early-age and long-term performance.

Accordingly, the project included two main tasks, which are presented in Chapters 2 and 3 of this report. Task 1 (Chapter 2) involved a quantitative evaluation of six potential mechanisms by which fly ash could control ASR in concrete materials containing glass fine aggregates. The mechanisms studied included: (1) alkali dilution, (2) alkali binding, (3) mass transport reduction, (4) increasing tensile strength, (5) altering ASR gel properties, and (6) reducing aggregate dissolution. Six fly ashes of different compositions (including four class F and two class C fly ashes) were studied to evaluate the effect of fly ash properties on its effectiveness against ASR. A variety of analytical tools were used to study the material's microstructure, its mechanical and transport properties, pore solution composition, aggregate dissolution rate, and ASR gel formation and composition.

Task 2 (Chapter 3) used the findings of Task 1 in mixture proportioning of concrete mixtures containing recycled glass sand. Most importantly, the effect of using glass sand on concrete strength is evaluated and proportioning charts were developed relating concrete's w/cm to its strength. In addition, other fresh

and hardened properties of three glasscrete mixtures were evaluated and compared with natural sand concretes with similar design strength or similar w/cm.

The outcomes of this research provide material/design engineers and concrete suppliers with much needed information to allow a safe and reliable use of recycled glass as an aggregate in Portland cement concrete. The main lessons learned, recommendations, and conclusions are provided in Chapter 4. The remainder of this chapter provides a brief literature review on the use of recycled glass aggregates in concrete.

1.3. Previous Work on Use of Recycled Glass Aggregates in Concrete

The traditional market for crushed recycled glass (cullet) is manufacturing new glass products; which primarily uses high-quality, color-sorted, and contamination-free cullet (Skumatz and Freeman 2007). Alternative markets for lower-grade cullet include applications as an abrasive, water filtration media, landscaping material, and as aggregate in construction including in pavement layers, in asphalt and concrete mixtures, and as a fill material. Application as concrete aggregates can be particularly rewarding since the high production volume of concrete materials can incorporate large quantities of recycled glass. Specifically in areas with limited availability of durable natural aggregates, recycled glass can be used as a partial aggregate replacement, thus reducing the cost and environmental impact of importing aggregates from elsewhere. For a more comprehensive discussion of the environmental and economic benefits of using recycled glass in concrete materials, please see Rajabipour et al. 2009.

Soda-lime glass is the most common type of glass used to produce containers and window plates. This type of glass contains a homogenous matrix of highly amorphous silicate. The typical chemical composition includes SiO_2 (>70%), Na_2O (~13%), and CaO (~11%). Since glass particles are crushed, they are angular and have residual intra-particle microcracks (Maraghechi et al. 2012). The use of crushed glass in architectural concrete panels dates back to the 1950s (Schmidt and Saia 1963). Unfortunately, many such panels have experienced cracking and spalling due to ASR (Mukherjee and Bickley 1986). The first report on using waste glass as coarse aggregate in concrete was published by Johnson (1974). This and a later report by Figg (1981) concluded that in many cases, the use of coarse glass aggregates resulted in considerable ASR expansion and cracking. In addition, these concretes showed poor workability, which resulted in inefficient compaction and low strengths.
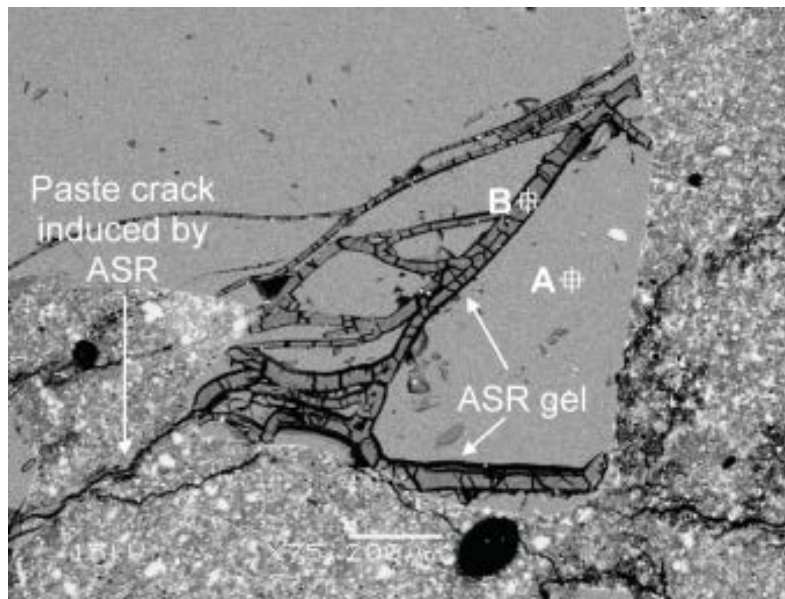

Figure 1-3: SEM image showing occurrence of ASR inside a glass particle and not at its interface (Rajabipour et al. 2010)

More recent research has examined the potential of using glass as fine aggregates in concrete. Polley et al. (1998) developed concrete mixtures with comparable strength to the control mixture without glass when they limited the glass particle size to 1.5 mm and glass content to 20% of the total concrete's aggregate. They also suggested the use of 25% fly ash to mitigate ASR. Based on the results of ASTM C1260 testing, Jin et al. (2000) reported that the ASR expansion of mortars containing soda-lime glass sand depends on the size of the glass particles. This and other studies (e.g., Zhu and Byars 2004) reported that larger glass particles are significantly more reactive than smaller particles. This trend is counterintuitive, as increasing the particle surface area should accelerate the reactions; assuming that ASR occurs at the glass-cement paste interface. Scanning electron microscopy (SEM) examination of ASTM C1293 and C1260 specimens affected by ASR revealed that glass particles do not undergo ASR at their surface. For example, Figure 1-3 shows an SEM micrograph of a glass particle that underwent alkali silica reaction through internal microcracks while the glass surface (i.e., interface with cement paste) remained intact. ASR initiates inside intra-particle cracks, which are originated during bottle crushing (i.e., they exist before glass is mixed in concrete). Larger particles contain wider cracks and a higher crack density, which result in a higher alkali silica reactivity (Maraghechi et al. 2012).

The hypothesis that residual bottle crushing cracks are responsible for ASR was validated by two further observations. First, soda-lime glass beads with the same oxide composition but no internal cracks were found to be innocuous when tested by ASTM C1260 (Rajabipour et al. 2012). Second, annealing (i.e., heat treatment) of crushed glass cullet to heal the residual cracks was found to mitigate ASR (Maraghechi et al. 2012). The reason that glass-paste interface is protected from ASR is not clearly understood, but may be related to the deposition of portlandite ($Ca(OH)_2$ abbreviated as CH), which favors a pozzolanic reaction (Hou et al. 2004). Evidence of pozzolanic reaction and C-S-H formation (i.e., calcium silicate hydrate gel, which is the main binding agent in concrete) at the interface has been observed using SEM with energy dispersive spectroscopy (EDS) (Rajabipour et al. 2010).

There is not sufficient experience in working with and testing the properties of concrete containing recycled glass aggregates. It is known that use of recycled glass may reduce the compressive strength of concrete (Rajabipour et al. 2009), but methods for proper mixture proportioning to achieve desired strength and workability have not been established. The effect of glass sand on other durability and hardened properties of concrete (e.g., resistance to chloride ion penetration) is unknown. This project was aimed at bridging such knowledge gaps.

1.4. Common Test Methods for Evaluating the Alkali Silica Reactivity of Concrete Aggregates

A variety of test methods are available to examine the potential reactivity of an aggregate source and to determine the required dosage of a certain pozzolanic materials, also known as supplementary cementitious materials (SCM), to be used in combination with a given reactive aggregate (Thomas et al. 2006, Lindgård et al. 2012). Among these, ASTM C1293 (concrete prism expansion test) has been suggested as the most reliable laboratory method to correctly replicate ASR that occurs in concrete structures in service, albeit at a moderately accelerated pace. In this test, the expansion of concrete prisms containing reactive coarse or fine aggregates is monitored over a 12-month period (24 months if SCMs are used). ASR is accelerated by boosting the mixture's alkali content and by maintaining the samples at 38 ^oC and 100% RH (relative humidity). The main drawback of this test is its duration (up to 24 months), which has prevented the widespread use of this test, especially for QC/QA applications to determine the durability of a concrete mixture when a new source of aggregates or a new source of SCM must be used.

Alternatively, the accelerated mortar bar test (ASTM C1260 or C1567) provides a highly accelerated test method to determine the potential ASR performance of combinations of SCMs and aggregates. In this test, mortar bars containing potentially reactive aggregates are submerged in a bath of 1M NaOH at 80 ^oC and their expansion is measured over a 2-week period. This test, too, has received its share of criticism, mainly because it exposes aggregates to an excessively harsh environment, and since the underlying ASR mechanisms may be different than those in field conditions. For example, unlike actual concrete structures whose pore solution alkalinity is dictated by the w/c, cement alkali content, and presence of SCMs; ASTM C1567 exposes mortar bars to rapid penetration of external alkalis, and as such, the results may be significantly affected by the mass transport properties of mortars (Shafaatian et al. 2012). Despite

these criticisms, ASTM C1567 has been shown to generally provide a conservative assessment of the ASR performance of mixtures containing SCM (Thomas et al. 2006). Based on published data for 70 different combinations of SCM and aggregates, Thomas and Innis (1999) concluded that the required dosage of SCM to produce <0.1% expansion in C1567 testing (and therefore passing this test) had a low risk of failing ASTM C1293. As such, and due to its time effectiveness, ASTM C1567 is currently widely used in North America and elsewhere to determine the required dosage of SCM for preventing ASR.

It is not clear why fly ash and other SCMs inhibit ASR in the ASTM C1567 test. Past research using field exposure and ASTM C1293 tests have suggested that fly ash mitigates ASR primarily through reduction of the concrete pore solution's pH through alkali dilution and binding (Thomas 2011). This conclusion, however, may not be directly applicable to ASTM C1567 mortars that are exposed to an "inexhaustible" source of external alkalis (Bleszynski and Thomas 1998), which may erase the beneficial effects of alkali dilution and binding. As such, to better understand the mechanisms leading to mitigation of ASR in ASTM C1567, this study performs a systematic evaluation of mortars containing fly ash and a highly reactive aggregate (soda-lime-silica glass).

References

- ACI 211.1-91, Standard Practice for Selecting Proportions for Normal, Heavyweight, and Mass Concrete, Reapproved 2009, American Concrete Institute, Farmington Hills, Michigan, USA
- ACI 318-11, Building Code Requirements for Structural Concrete, 2011, American Concrete Institute, Farmington Hills, Michigan, USA
- ASTM C618-08a, Standard Specification for Coal Fly Ash and Raw or Calcined Natural Pozzolan for Use in Concrete, 2008, American Society for Testing and Materials, West Conshohocken, Pennsylvania, USA
- ASTM C1260-07, Standard Test Method for Potential Alkali Reactivity of Aggregates (Mortar-Bar Method), 2007, American Society for Testing and Materials, West Conshohocken, Pennsylvania, USA
- ASTM C1293-08b, Standard Test Method for Determination of Length Change of Concrete Due to Alkali-Silica Reaction, 2008, American Society for Testing and Materials, West Conshohocken, Pennsylvania, USA
- ASTM C1567-07, Standard Test Method for Determining the Potential Alkali-Silica Reactivity of Combinations of Cementitious Materials and Aggregates (Accelerated Mortar-Bar Method), 2007, American Society for Testing and Materials, West Conshohocken, Pennsylvania, USA
- R.F. Bleszynski, M.D.A. Thomas, Microstructural studies of alkali-silica reaction in fly ash concrete immersed in alkaline solutions, Advanced Cement Based Materials, 1998, 7(2), 66-78
- J.W. Figg, Reaction between cement and artificial glass in concrete, 5th International Conference on Concrete Alkali Aggregate Reactions (ICAAR), (1981) Cape Town, South Africa, S 252-257.
- K.J. Folliard, M.D.A. Thomas, B. Fournier, K.E. Kurtis, J.H. Ideker, Interim Recommendations for the Use of Lithium to Mitigate or Prevent Alkali-Silica Reaction, FHWA Report# FHWA-HRT-06-073, Federal Highway Administration, Washington, DC, USA
- L.J. Hanle, K.R. Jayaraman, J.S. Smith, CO_2 emissions profile of the U.S. cement industry, U.S. Environmental Protection Agency, www.epa.gov/ttnchie1/conference/ei13/ghg/hanle.pdf (accessed 04.27.2012)
- X. Hou, L.J. Struble, R.J. Kirkpatrick, Formation of ASR gel and the role of C-S-H and portlandite, Cement and Concrete Research, 2004, 34, 1683-1696.
- W. Jin, C. Meyer, S. Baxter, Glascrete – Concrete with Glass Aggregate, ACI Materials Journal, 97(2) (2000) 208-213
- C.D. Johnson, Waste glass as coarse aggregate for concrete, Journal of Testing and Evaluation, 2(5) (1974) 344-350
- S.H. Kosmatka, M.L. Wilson, Design and Control of Concrete Mixtures, 15th Ed., 2011, Portland Cement Association, Skokie, Illinois, USA
- J. Lindgård, Ö. Andiç-Çakır, I. Fernandes, T. F. Rønning, M. D. A. Thomas, Alkali–silica reactions (ASR): Literature review on parameters influencing laboratory performance testing, Cement and Concrete Research, 2012, 42, pp. 223–243
- H. Maraghechi, S. Shafaatian, G. Fischer, and F. Rajabipour, The role of residual cracks on alkali silica reactivity of recycled glass aggregates, Cement and Concrete Composites, 34 (2012) 41-47

- S. Mindess, J.F. Young, D. Darwin, Concrete, 2nd Ed., 2003, Pearson Education, Upper Saddle River, New Jersey, USA
- P.K. Mukherjee, J.A. Bickley, Performance of glass as concrete aggregates". 7th International Conference on Concrete Alkali Aggregate Reactions (ICAAR), 1986, Ottawa, Canada, 36-42.
- Municipal Solid Waste Generation, Recycling, and Disposal in the United States: Facts and Figures for 2010. US Environmental Protection Agency (EPA), Solid Waste and Emergency Response: www.epa.gov/osw, Washington, DC, November 2011
- Owens-Illinois Inc. Glass Cullet Stockpile in Huntington, West Virginia, Photographed 1993, www.corbisimages.com/stock-photo/rights-managed/JA004525/bucket-loader-at-green-glass-stockpile?caller=search (accessed May 2012)
- C. Polley, S.M. Cramer, R.V. de la Cruz, Potential for using waste glass in portland cement concrete, ASCE Journal of Materials in Civil Engineering, 10 (4) (1998) 210-219
- F. Rajabipour, G. Fischer, P. Sigurdardottir, S. Goodnight, A. Leake, E. Smith, Recycling and utilizing waste glass as concrete aggregate, Proceedings of TRB Annual Meeting, 2009, CD-Rom Paper# 09-2195, Transportation Research Board, Washington, DC, USA
- F. Rajabipour, H. Maraghechi, G. Fischer, Investigating the Alkali-Silica Reaction of Recycled Glass Aggregates in Concrete Materials, Journal of Materials in Civil Engineering, 22(12) (2010) 1201-1208
- F. Rajabipour, H. Maraghechi, S.M.H. Shafaatian, Mechanisms of ASR and Its Mitigation by Fly Ash in Mortars Containing Recycled Glass Aggregates , 2012, 14th International Conference on Concrete Alkali Aggregate Reactions (ICAAR), Austin, Texas
- J. Reindl, Reuse/Recycling of Glass Cullet for Non-Container Uses, 2003, www.epa.gov/osw/conserve/rrr/greenscapes/pubs/glass.pdf (accessed April 2012)
- A. Schmidt, W.H.F. Saia, Alkaline aggregate reaction tests on glass used for exposed aggregate wall panel work, ACI Materials Journal, 60 (1963) 1235-1236
- S.M.H. Shafaatian, H. Maraghechi, F. Rajabipour, Assessing the role of ion transport in mitigation of ASR by fly ash in accelerated mortar bar test, Submitted to ASCE Journal of Materials in Civil Engineering, 2012
- L.A. Skumatz, J. Freeman, What do we do with these piles?, Resource Recycling, June 2007
- M.D.A. Thomas, F.A. Innis, Use of the accelerated mortar bar test for evaluating the efficacy of mineral admixtures for controlling expansion due to alkali-silica reaction, Cement, Concrete and Aggregates, 1999, 21(2), pp. 157-164
- M.D.A. Thomas, B. Fournier, K. Folliard, J. Ideker, M. Shehata, Test methods for evaluating preventive measures for controlling expansion due to alkali–silica reaction in concrete, 2006, Cement and Concrete Research, 36(10),pp. 1842–1856
- M.D.A. Thomas, The effect of supplementary cementing materials on alkali-silica reaction: A review, Cement and Concrete Research, 2011, 41, 209-216
- U.S. Geological Survey, Mineral Commodity Summaries, January 2012, http://minerals.usgs.gov/minerals/pubs/mcs/2012/mcs2012.pdf
- H. Zhu, E.A. Byars, Alkali-silica reaction of recycled glass in concrete, 12th International Conference on Concrete Alkali Aggregate Reactions (ICAAR), (2004) Beijing, China, 811-820

CHAPTER 2:
MECHANISMS OF ASR MITIGATION BY FLY ASH

2.1.   Introduction

Alkali silica reaction (ASR) in concrete is a deleterious mechanism in which the amorphous silicate structure of a reactive aggregate (e.g., recycled glass) dissolves in the high alkaline pore solution of concrete and coagulates in the form of a colloidal silica gel, which absorbs water and swells (Swamy 1992, Hobb 1988). The resulting tensile stresses lead to cracking of concrete. Literature on mitigation of ASR for natural aggregates is extensive and in particular, it has been shown that coal fly ash is effective in controlling the damage (Diamond 1981, Dunstan 1981, Hobbs 1982, Hobbs 1986, Carrasquillo and Snow 1987, Nagataki et al. 1991, Chen et al. 1993, Berra et al. 1994, Hobbs 1994, Shayan et al. 1996, Thomas 1996, Duchesne and Bérubé 2001). However, there is limited understanding of how fly ash mitigates ASR, especially in concretes containing recycled glass. Such understanding can result in identifying fly ash properties (e.g., oxide compositions) that determine its effectiveness against ASR and could ultimately assist material engineers in better selection and proportioning of fly ash for concretes containing reactive aggregates. The goal of this chapter is to expand the knowledge related to the ASR mitigation capacity of fly ash by studying mixtures tested according to ASTM C1567, the accelerated mortar bar test. In addition, the results can shed light on the material properties of mortars that most significantly impact the results of ASTM C1567 test.

2.2.   Existing Literature

Prior studies have mentioned six potential mechanisms for mitigation of ASR by fly ash: alkali dilution, alkali binding, limiting mass transport, improving strength, modifying ASR gel, and consumption of portlandite. A brief description of each mechanism is provided below.

(1) Alkali dilution: the alkalinity of concrete's pore solution is reduced by replacing cement with fly ash (Diamond 1981, Hobbs 1982). The pore solution of concrete has a high pH (>12.5) due to the presence of solid $Ca(OH)_2$ as well as the dissolution of alkali sulfates (e.g., Na_2SO_4, K_2SO_4) from cement particles (Rajabipour et al. 2008). Even when the alkali (Na_2O_{eq}) content of fly ash is higher than that of cement, the dilution effect is observed as only a portion of fly ash alkalis are soluble per ASTM C311 test (Hobbs 1988); and even that portion dissolves very slowly in the pore solution (Diamond 1981).

(2) Alkali binding: the additional pozzolanic C-S-H is able to bind alkali ions and remove them from the pore solution (Canham et al. 1987, Duchesne and Bérubé 1994). Pozzolanic reaction is a chemical reaction between the excess portlandite (CH) and the amorphous silicates provided by fly ash or other pozzolanic materials. The main product of a pozzolanic reaction is formation of C-S-H, which is the main binding phase in concrete (Mindess et al. 2003). In addition to increasing the volume fraction of C-S-H, the pozzolanic C-S-H has a lower C/S and shows a higher alkali binding capacity in comparison with C-S-H from cement hydration (Rayment 1982, Thomas 2011). This may be attributed to increasing the acidity of silanol (Si-OH) groups (Hong and Glasser 1999) or developing alkali attractive (i.e., negative) surface charges on the low C/S C-S-H (Monteiro et al. 1997). In addition, the alumina in fly ash can be incorporated into pozzolanic reactions to form C-A-S-H gel with a considerably higher binding capacity than C-S-H (Hong and Glasser 2002). Based on the results of ASTM C1293 testing, pore solution alkalinity of concrete has a strong correlation with ASR prism expansions (Shehata and Thomas 2000). Fly ashes with high Na_2O_{eq} and CaO contents have been found to be less efficient in reducing pore solution alkalinity, and also less effective in controlling ASR (Canham et al. 1987, Shehata and Thomas 2006).

(3) Limiting mass transport: pozzolanic reactions can, over time, reduce the mass transport properties of concrete (Swamy et al. 1992, Lothenbach et al. 2011). A reduction in ion diffusion coefficient is significant, especially where an external source of alkalis is present (e.g., in ASTM C1567). In addition, reduction in hydraulic permeability of concrete can slow down the absorption of water and swelling of the ASR gel. Despite the importance of mass transport for long-term measurements, the significance of this mechanism for accelerated tests is unclear. Fly ash generally reacts slower than Portland cement and it

is reported that concrete containing fly ash has higher porosity and transport properties at early ages in comparison with 100% Portland cement concrete (Pandey and Sharma 2000, Li et al. 2006).

(4) Improving tensile strength: fly ash concrete, over time, develops a higher tensile strength, which aids in resisting internal stresses and cracking (Swamy et al. 1992). Again, it is unclear whether the tensile strength is improved or reduced at early ages due to slow reactivity of fly ash.

(5) Modifying ASR gel properties: by changing the composition of ASR gel, fly ash may reduce the swelling capacity, swelling pressure, and viscosity of ASR gel. Monteiro et al. (1997) observed that high CaO/Na_2O_{eq} gels have lower swelling capacity than gels with low CaO/Na_2O_{eq}. Struble and Diamond (1981) reported that calcium-free sodium-silicate gels can become fluid (i.e., lose their viscosity) under moderate pressures, unlike calcium-rich gels, which remain solid. Similarly, Bleszynski and Thomas (1998) observed that very low CaO/Na_2O_{eq} gels can diffuse freely into surrounding cement paste without exerting damage, which may indicate their low viscosity and swelling pressure. Bonakdar et al. (2010) related ASR gel composition to the number of bridging oxygens in silica tetrahedra and reported that gels produced in a less basic environment (i.e., fly ash) have a fibrous structure, which results in limited swelling pressure in comparison with the 3-dimensional structure gels formed without fly ash.

(6) Consumption of portlandite: it has been suggested that the presence of free $Ca(OH)_2$ is necessary for formation of expansive ASR gels at the perimeter of reactive aggregates (Chatterji 1979, Bleszynski and Thomas 1998). As a result, consumption of portlandite by the pozzolanic reaction of fly ash may reduce the tensile stresses resulting from formation and swelling of the ASR gel. Portlandite can also serve as a pH buffer to maintain the pore solution's pH above 12.6.

This project investigates the contributions of different mechanisms leading to mitigation of ASR by fly ash in the ASTM C1567 test. Out of the six potential mechanisms described above, the first five are considered in this work. Since recycled glass aggregates do not undergo ASR at their surface, where CH is confirmed by SEM to be present, it was decided to exclude the portlandite consumption mechanism from this study. The authors are currently performing a parallel study dedicated to better understanding the role of CH on alkali-silica reaction. In addition, a new hypothesis is proposed and evaluated in this work: "The presence of fly ash (or other SCMs) significantly increases the available surface area of amorphous silicates in the system. Since such surfaces attract the damaging OH- ions; at a given pH, the concentration of OH^- ions attacking a unit surface area of siliceous aggregates will be reduced. This results in reducing the dissolution rate of the aggregates." This hypothesis, if validated, can serve as a new mechanism for ASR mitigation by siliceous SCMs.

2.3   Materials and Methods

Mortar mixtures were prepared according to the proportions of ASTM C1567 using pulverized recycled glass sand and a mixture of Portland cement and fly ash as binder. ASTM C150 type I Portland cement was used. Six ASTM C618 fly ashes were studied, including four class F (identified as F1, F2, F3, F4) and two class C (identified as C1, C2). Fly ashes were used at different cement replacement levels (mass based) to evaluate their efficiency in controlling ASR. A control mortar containing 100% Portland cement was also tested. The oxide composition of cement, glass, and all fly ashes are presented in Table 2-1. Recycled glass sand was composed of three main colors: amber (~30%), clear (~30%) and green (~40%). Glass bottles were washed and crushed using a ball mill. All mortars were prepared with w/cm = 0.47, and 53% volume fraction of sand with gradation in the range 4.75 mm to 150 μm according to ASTM C1567. Mortars were mixed according to ASTM C305. Specimens were prepared and moist cured for 24 hours at 23 °C. After 24 hours, the specimens were demolded and cured submerged in water at 80 °C for another 24 hours. Finally, the specimens were transferred to a 1 M NaOH bath at 80 °C and maintained for 14 days. The following tests were performed subsequently.

2.3.1   Accelerated mortar bar test (ASTM C1567)

This test was used to determine the dosage of each type of fly ash needed to reduce the mortar bar expansion below the threshold of 0.1%. A total of 56 different mixtures were tested. For each mixture, four 25×25×250mm prisms were prepared with embedded gage studs at the ends to facilitate length measurements. A digital comparator with accuracy to 0.0025 mm was used. Prism lengths were

measured after demolding, 24 hours of water curing, and 1, 3, 5, 7, 10, and 14 days' submersion in an NaOH bath.

Table 2-1: Oxide composition (wt %) of Portland cement, glass, and fly ashes

OXIDE	CEMENT	GLASS	F1	F2	F3	F4	C1	C2
CaO	62.50	10.62	2.42	1.26	3.81	13.52	26.63	27.33
SiO_2	19.90	73.13	51.75	59.93	49.20	52.23	33.48	34.02
Al_2O_3	5.44	1.99	33.70	24.97	23.34	16.36	18.59	18.74
Fe_2O_3	2.26	0.52	4.08	6.33	14.72	5.78	6.13	5.86
Na_2O	0.30	13.74	0.40	0.36	0.69	2.82	0.37	1.50
K_2O	0.89	0.34	1.16	1.90	1.78	2.16	0.72	0.35
MgO	2.31	0.53	0.60	1.00	1.03	4.30	1.48	5.00
MnO	0.09	N/D*	0.03	0.07	0.03	0.05	0.03	0.05
TiO_2	0.29	N/D*	1.30	1.48	1.03	0.64	1.95	1.57
SO_3	4.93	N/D*	0.25	1.33	1.47	1.17	7.65	3.67
P_2O_5	0.23	N/D*	0.30	0.28	0.35	0.18	0.26	1.03
LOI	0.86	---	4.01	1.09	2.55	0.80	2.71	0.88
C/S	3.14	0.19	0.05	0.02	0.08	0.26	0.80	0.80
Na_2O_{eq}	0.89	13.96	1.16	1.61	1.86	4.24	0.84	1.73

*N/D is not detected

2.3.2   Pore solution extraction and analysis

To investigate the impact of fly ash on pore solution ion concentrations, and to quantify the extent of alkali dilution, binding, and transport, pore solution of the control (100% PC), 15% F1 and 35% C2 mortars were extracted.   The latter two mortars contained sufficient fly ash to pass the ASTM C1567 test (expansion<0.1%).   Pore solution extraction was performed immediately after mixing, after demolding (24h), and at 0, 3, 7, and 14 days of NaOH bath exposure. Pore solution of plastic mortar was extracted by pressure filtration using nitrogen gas. For hardened samples, mortar prisms were removed from the baths, surface dried, broken into smaller pieces, and then pressurized inside a pore solution extraction die up to a maximum stress of 550 MPa at a controlled rate of 75 MPa/min. The extracted solutions were collected in sealable PP vials, filtered through 0.2 μm PTFE membrane filters, and immediately tested by HCl titration to measure [OH⁻].   The concentrations of other elements (Na, K, Ca, Si, Al, and S) were measured using a Perkin-Elmer Optima 5300 ICP-AES.

2.3.3   Measurement of ion diffusivity using electrical impedance spectroscopy

The ion diffusion coefficient of mortars (D, m^2/s) was determined using non-destructive electrical conductivity measurements according to the Nernst-Einstein equation (Garboczi 1990):

$$D = D_o \frac{\sigma}{\sigma_0}$$

(2-1)

Where σ (S/m) is the electrical conductivity of mortar, σ_o(S/m) is the conductivity of pore solution, and D_o (m^2/s) is the diffusion coefficient of ion in pore solution. For information on the scientific basis of this method and details of measurements and data interpretation, please see Christensen et al. (1994), Akhavan and Rajabipour (2012), and Shafaatian et al. (2012). Samples from three mortars were tested: control, 15% F1, and 35% C2. The electrical conductivity of mortars (σ) was measured between a pair of 3.2-mm-diameter stainless steel electrodes embedded through the thickness of each mortar bar at 15 mm distance between the centers of electrodes.   The bulk resistance was measured using an HP-4194A impedance analyzer in frequency sweep mode (40 Hz to 10 MHz) and using 250 mV voltage. The results were converted to electrical conductivity using an experimentally established geometry factor (Rajabipour 2006). The measurements were performed after 0, 3, 7, and 14 days of mortar exposure to NaOH bath. An average of four measurements obtained from four duplicate specimens was used to establish each data point. In parallel, pore fluids of mortars were extracted (as described above) and their electrical conductivity (σ_o) was measured using a commercial conductivity probe. The value of ion diffusivity of

pore solution was assumed to be $D_o=1.065\times10\text{-}9$ m^2/s for NaOH in water at 80 ^{o}C (CRC Handbook 2010). This value corresponds to the effective self diffusion coefficient of NaOH that is calculated according to the formula by the CRC Handbook (2010) using the diffusivity of Na$^+$ and OH$^-$ ions. The self-diffusion coefficient does not consider the ionic strength of the pore solution.

2.3.4   Tensile and compressive strength tests

To examine the effect of fly ash on tensile strength (i.e., modulus of rupture) of mortars, 25×25×250 mm prisms were tested in 3-point bending. Specimens were prepared according to ASTM C1567 and using a dosage of each fly ash that controlled expansions to below 0.1%: 15% F1, 15% F2, 20% F3, 20% F4, 25% C1 and 35% C2. Prisms were tested after 3 days' exposure to the NaOH bath. ASTM C1567 measurements showed expansions starting in the controlled (100% PC) mortar after 3 days' NaOH exposure. As such, this time was chosen as the onset of cracking. Prisms were tested using a displacement-controlled setup that applied a mid-span deformation of 5µm/sec until failure. The compressive strength of similarly cured mortar cubes (50×50×50 mm) was tested according to ASTM C109. For both tensile and compressive strength tests, an average of three measurements was used per each mixture.

2.3.5   SEM/EDS imaging

SEM/EDS imaging was used to study the microstructure of the mortars, and to study ASR gel formation and composition. Imaging was performed on the control, 15% F1, and 35% C2 mortars. After 7 and 14 days of NaOH exposure, cross sections were saw-cut from mortar bars with approximate thickness of 1 cm. Specimens were vacuum dried inside a desiccator for 48 hours and then impregnated with a low-viscosity epoxy. After setting, the epoxy was polished off and the specimens were successively polished with 30, 15, 9, 6, 3, and 1 µm grits. Polishing oil was used instead of water to prevent leaching. The specimens were carbon coated prior to SEM. Image acquisition was performed in backscatter (BSE) mode using an FEI Quanta 200 environmental SEM (ESEM) instrument with a lateral resolution of 3.5 nm. The ESEM was equipped with an X-ray energy dispersive spectroscopy (EDS) detector for compositional analysis. EDS spot analysis was performed on at least 20 ASR gel points for the control, 15% F1 and 35% C2 mortar cross sections to gain information regarding the composition of ASR gels. The gel composition was examined after 7 and 14 days of NaOH exposure to monitor changes in its composition over time.

2.3.6   Aggregate dissolution rate measurements

To assess the dissolution rate of glass aggregates in the presence or absence of fly ash, a glass corrosion experiment was performed. Soda-lime glass slides (75×25×1 mm) were submerged in a 340 ml 1 M NaOH solution at 80 °C for a period of 14 days. Solutions were not stirred during the experiment. Periodic mass-loss measurements from glass slides were used to monitor the dissolution rate of glass. For each measurement, the glass slides were removed from the solution, and the silica gel formed on the surface of each slide was carefully washed off by de-ionized water. Mass measurements were performed using a balance with accuracy of 0.0001 g. For each data point, measurements were obtained from two duplicate slides. The corrosion experiments were performed in the absence of fly ash, and also for systems where 10 g or 20 g of F1 fly ash was added to the solution. The corrosion tests were performed inside sealable plastic containers to minimize evaporation and carbonation. The [OH$^-$] was periodically monitored by sampling the solution and performing acid titration.

2.4   Numerical Model to Simulate Alkali Transport and Binding

A numerical model was developed to assess the simultaneous effects of ion diffusion and binding on pore fluid concentration of mortars during the ASTM C1567 test. Several simplifying assumptions were made in the development of this model, as described below. As such, the results only provide a semi-quantitative evaluation of the relative significance of ion diffusion and binding, and should not be directly/numerically compared with pore fluid compositions of mortars that were measured experimentally (section 2.5.2).

A 1D finite-difference model was developed to simulate the diffusion of NaOH from the soak solution by solving Fick's 2nd law. The alkali binding effect was accounted for by introducing a sink term in the model. Ion diffusion was simulated within a mortar cross section of 25×25 mm^2 that was exposed to 1 M

NaOH from two opposite faces (Figure 2-5). The other two faces were considered as sealed (1D model). Mortar diffusion coefficients were obtained experimentally (section 2.5.3) at the time of submerging samples into the NaOH bath (2 days after casting). For the 100% PC mortar, D = 1.16×10^{-11} m^2/s and for the 15% F1 mortar, D = 3.02×10^{-12} m^2/s was used. Diffusion coefficients were assumed to remain constant during the simulations. Diffusivity of NaOH in pore solution (D_o) at 80 ^{o}C was used as 1.065×10^{-9} m^2/s (CRC Handbook 2010), without considering the effect of ion activity coefficients. The model included a sink term to account for alkali binding by C-S-H according to the distribution ratio (Hong and Glasser 1999):

$$Rd = \frac{\text{[Na] in solid C-S-H (Mol/kg)}}{\text{[Na] in pore solution (Mol/kg)}} \qquad (2-2)$$

The values of Rd used in the model were a function of Ca/Si of C-S-H according to the work of Hong and Glasser (1999). For 100% PC mortar (Ca/Si=1.87), Rd = 0.5, and for 15% F1 mortar (Ca/Si=1.39), Rd = 1.25 were used. This suggests a better binding capacity for mortars containing fly ash. The Ca/Si was determined by EDS of C-S-H phase in 100% PC and 15% F1 mortars. At least 20 EDS spot analyses were perfomed on C-S-H rims around cement and fly ash particles; and the average Ca/Si was obtained. The mass fraction of C-S-H was assumed to be the same for both 100% PC and 15% F1 pastes ($m_{C-S-H} \approx$ 50% wt. of each paste). At every time step (Δt=15 min), sodium concentration ([Na]) in pore solution was calculated based on Fick's law. Subsequetntly, [Na] in pore solution was adjusted by subtracting the amount that can be absorbed by the solid phase according to Eq. (2-2). The model then proceeded to the next time step and the simulation continued.

The pore solution was assumed to only contain Na and OH ions; as such, multi-ion diffusion was ignored. At every point within the pore solution, charge neutrality was maintained, meaning: [Na$^+$]=[OH$^-$]. Initial condition was defined as [OH$^-$]=0.23M across the thickness of mortar for both control and fly ash mortars. This value reflects the [OH$^-$] for the control mortar at 48 hours after casting and before exposure to NaOH (Figure 2-3(a)). The 15% F1 mortar showed smaller [OH$^-$] at this time; however, the same value of [OH$^-$]=0.23M was chosen in the simulation of both mortars so the final results exclusively represent the contribution of NaOH diffusion and binding during the 14-day bath exposure period. Further OH$^-$ release due to continued hydration of cement and fly ash beyond 48 hours was assumed negligible. The model's boundary condition was [OH-] =1.0 M at 0 and 25 mm (i.e., the bath concentration).

2.5   Results and Discussion

2.5.1   Sufficient dosage of fly ash to mitigate ASR
The 14-day expansion of mortar bars in the ASTM C1567 test is presented in Figure 2-1. This figure can be used to determine the minimum replacement level of each fly ash to control expansions below the 0.1% threshold: 15% F1, 20% F2, 20% F3, 25% F4, 25% C1 and 35% C2. The oxide compositions of the cement and six fly ashes are shown in the ternary phase diagram of Figure 2-2 (oxide contents were normalized by subtracting the values for SO$_3$ and LOI). By comparison of Figures 2-1 and 2-2, it is evident that fly ashes with higher contents of CaO$_{eq}$ are less effective in mitigating ASR. This may be due to inefficiency of such ashes in reducing the alkalinity of pore fluid of mortars, as suggested by Shehata and Thomas (2000) and Malvar and Lenke (2006). Figure 2-2 also shows the oxide contents of composite binders that were able to mitigate ASR (e.g., 85% PC+15% F1, 80% PC+20% F2, etc.). Interestingly, all composite binder points are clustered in one area of the phase diagram below a CaO$_{eq}$ value of 61%. It would be interesting to test other combinations of different cements and fly ashes to determine if a maximum CaO$_{eq}$ threshold of ~60% is sufficient in controlling ASR for mortars containing recycled glass sand. In addition, it is important to determine the role of Al$_2$O$_{3eq}$; at similar CaO$_{eq}$, would ashes with higher contents of Al$_2$O$_3$ and Fe$_2$O$_3$ be more efficient in ASR mitigation? Of course, other parameters such as fly ash particle size and crystal content also affect its efficiency against ASR. In the present work, the six fly ashes had comparable particle size distributions as quantified by laser diffraction.
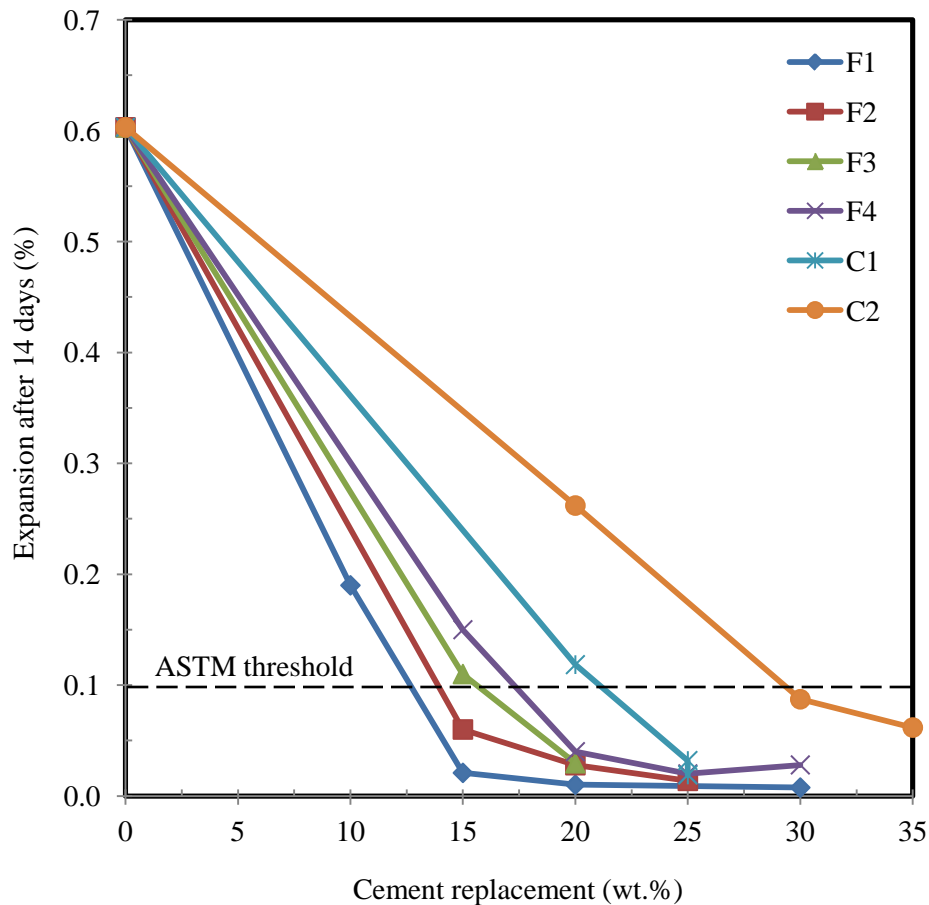
Figure 2-1: Results of ASTM C1567 showing ASR expansions as a function of fly ash type and dosage

2.5.2   Pore solution composition

The results of pore solution analysis are presented in Figures 2-3(a-c). Figure 2-3(a) shows hydroxyl ion concentration ($[OH^-]$) over the duration of the ASTM C1567 test. At 0d, all 3 mortars have $[OH^-] \approx 100$ mM; despite higher Na^2O_{eq} of both fly ashes compared with PC. Note that fly ash alkalis may dissolve more slowly than those of cement due to the slow reactivity of fly ash. During the first 24 hours, concentrations rose mainly due to cement hydration. At 24 h, the $[OH^-]$ of fly ash mortars was 22% and 34% less than the control mortar, which shows the effect of alkali dilution. During the next 24 hours, mortars were submerged in a water bath at 80 ^{o}C, which promoted leaching of alkalis. The rate of leaching was proportional to the ion diffusivity of mortars and was the highest for 100% PC. At 48 h, the $[OH^-]$ had dropped to 170 to 270 mM and the effect of alkali dilution was nearly totally erased. During the next 14 days, $[OH^-]$ of mortar pore solutions increased steadily due to exposure to the NaOH bath. The control mortar showed the highest concentrations, which agrees with its high ion diffusion coefficient (section 2.5.3). As the dissolution rate of glass aggregates is strongly related to $[OH^-]$, the highest rate of ASR was observed in the 100% PC mortar. At the test's conclusion, the $[OH^-]$ in the control mortar reached and surpassed the OH^- concentrations of the soak solution (1M). This is due to an ion exchange mechanism that occurs when the silicate glass or silicate gel contain alkalis (Clark and Yen-Bower 1980):

$$\equiv Si\text{-}ONa + H_2O \rightarrow \equiv Si\text{-}OH + Na^+ + OH^- \tag{2-3}$$

This reaction results in hydrolysis of water, and an increase in both $[Na^+]$ and $[OH^-]$ of pore solution. This is further discussed in section 2.5.7.
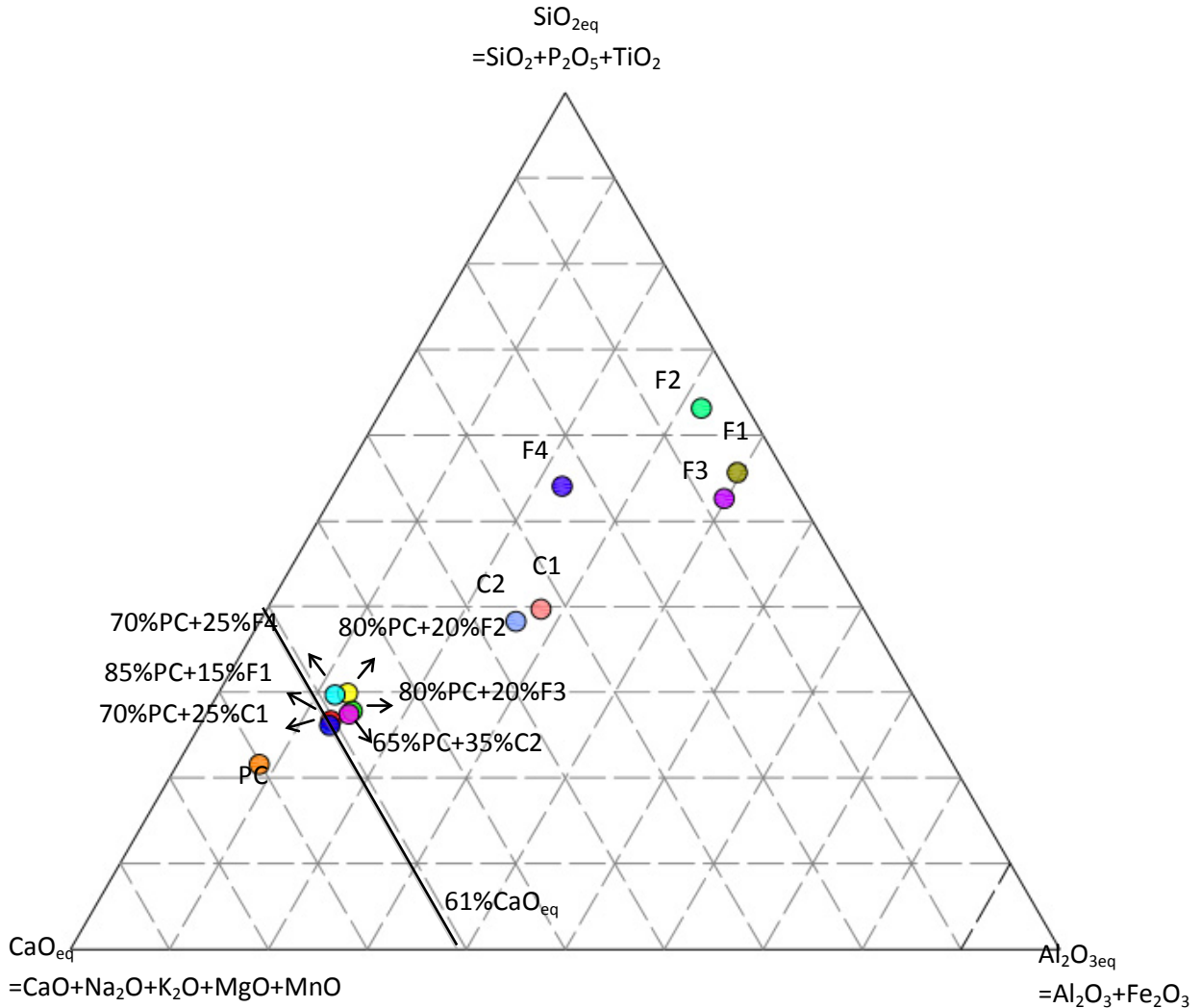
Figure 2-2: Ternary phase diagram showing cement and fly ash compositions

Figure 2-3(b) shows variations in elemental [Na] in the pore solution of the three mortars. It must be noted that ICP measures the total [Na], which is not the same as ionic [Na$^+$]. In pore solutions studied here, silica gel globules (<0.2 μm) are present in the pore solution and these can contain non-ionic Na in their structure. These globules have been dissolved from the soda-lime glass aggregates. As a result, it should not be surprising that [OH$^-$] does not necessarily equal [Na]+[K].

Immediately after mixing, [Na] was in the range 78 to 138 mM, with the 100% PC mortar showing the highest concentration. During the first 48 hours, [Na] in all three mortars increased steadily due to reaction of the cement and fly ash. At 48 h, [Na] in 35% C2 mortar was 333 mM in comparison with 231 and 202 mM for the other mortars. This is likely due to a significantly higher Na$_2$O of C2 fly ash (see Table 2-1). Interestingly, the water curing period (between 24 and 48 hours) did not result in reduction of [Na], unlike the trend observed for [OH$^-$] and [K]. After submersion of the mortar prisms inside 1 M NaOH, the Na content of pore solutions increased by a factor of up to 5.8 times. This increase was more rapid in the 100% PC mortar, which agrees well with its higher ion diffusion coefficient as discussed in the next section.
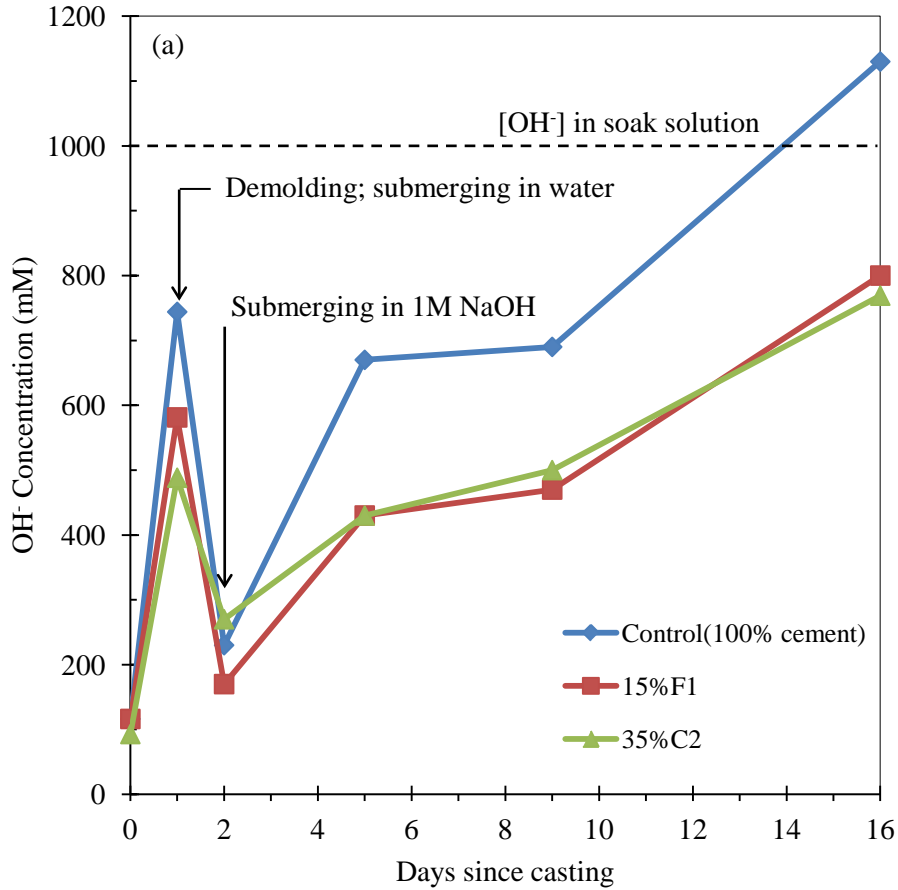
14

Figure 2-3: Pore solution composition of mortars during ASTM C1567 test: (a) [OH-] ion

Finally, the concentrations of potassium (K) in the three pore solutions are shown in Figure 2-3(c). Significant differences in the initial [K] are observed due to potassium dilution of the fly ashes. Although the K_2O content of F1 fly ash is higher than PC (1.16% vs. 0.89%), the 15% F1 mortar shows 43% less [K] at 0 day due to a slower reaction and release of alkalis by fly ash. During the first 24 hours, [K] increases in all three mortars. During the water curing period (between 24 and 48 hours), potassium content drops by leaching out of the mortars. At 48 hours, [K] in the 100% PC mortar is 224 mM, compared with 171 mM and 129 mM for the fly ash mortars. During the next 14 days, where mortars were submerged in NaOH bath, potassium leaching continued, albeit at a slower rate. The control mortar showed a faster rate of K leaching, in agreement with its higher ion diffusivity.
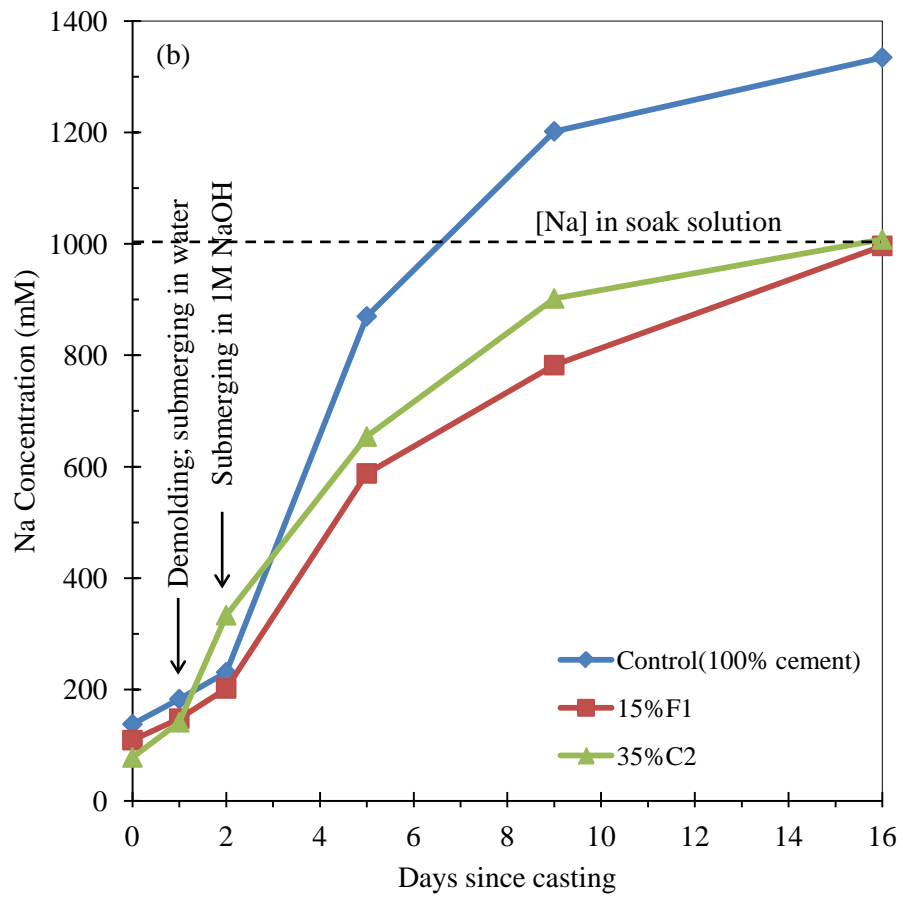
Figure 2-3: Pore solution composition of mortars during ASTM C1567 test: (b) [Na] element
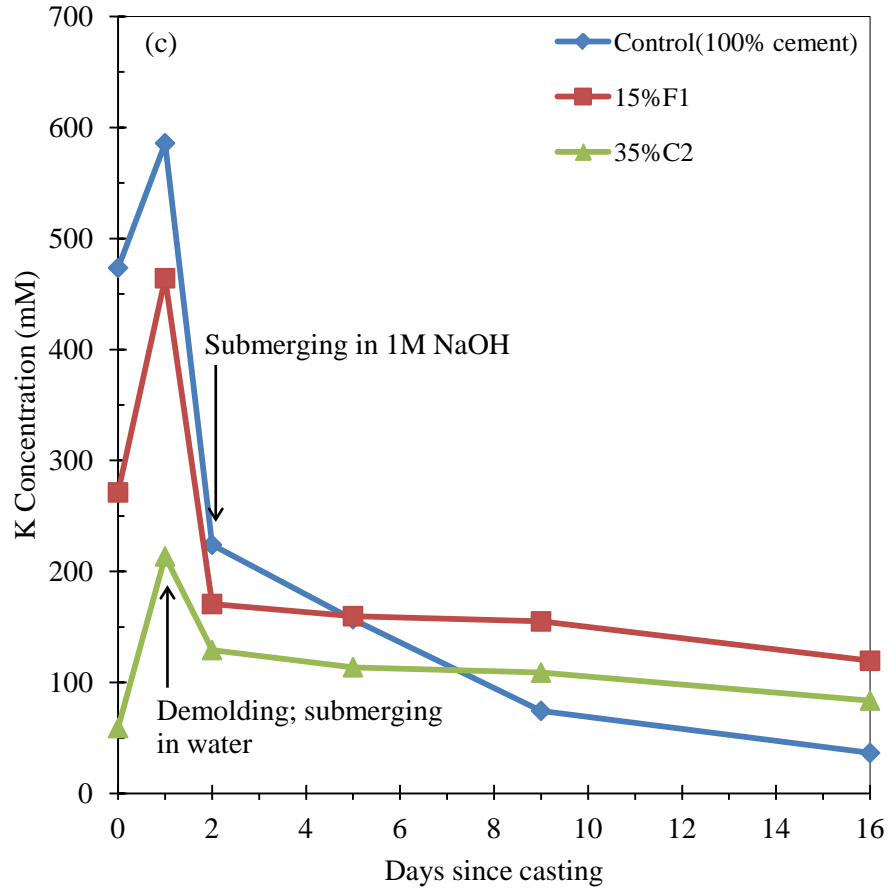
Figure 2-3: Pore solution composition of mortars during ASTM C1567 test: (c) [K] element

2.5.3 Ion diffusion coefficient

The ion diffusion coefficient of mortars was measured using electrical impedance spectroscopy and according to the Nernst-Einstein equation (2-1). Figure 2-4 shows the results for the control, 15% F1, and 35% C2 mortars over the duration of the ASTM C1567 test. The control mortar shows a significantly larger (by a factor of 4 to 7) ion diffusivity than the two fly ash mortars. This means that NaOH can penetrate much faster through the 100% PC mortar (in agreement with pore fluid analysis data of Figure 2-3), which in turn results in significantly larger ASR expansions (Figure 2-1). As reported by Shafaatian (2012), and in agreement with the results of Pandey and Sharma (2000) and Li et al. (2006), while the fly ash mortars show slightly higher porosity, their lower ion diffusivity is the result of a considerable reduction in the pore size and a significant increase in the tortuosity of the pore network.

These findings strongly support the role of fly ash in reducing ion transport as a major mechanism by which fly ash mitigates ASR during ASTM C1567 testing. It was observed that even after 48 hours since casting, fly ash mortars can show a considerably lower diffusion coefficient. Note that these mortars are water cured for 24 hours at 80 ^{o}C which can drastically boost the reactivity of fly ash. It is also observed in Figure 2-4 that the diffusivity of the control mortar increases up to 9 days but subsequently decreases. To make sure that this is not an experimental error, the tests were repeated and similar results were obtained. The initial increase in diffusivity is probably due to microcracking caused by ASR. As these cracks are filled by ASR gel (with much lower electrical conductivity and ion diffusivity than the pore solution), the overall conductivity/diffusivity of the mortar decreases. The diffusivity of the fly ash mortars remained relatively constant during the test period. This further implies a low level of microcracking in fly ash mortars.
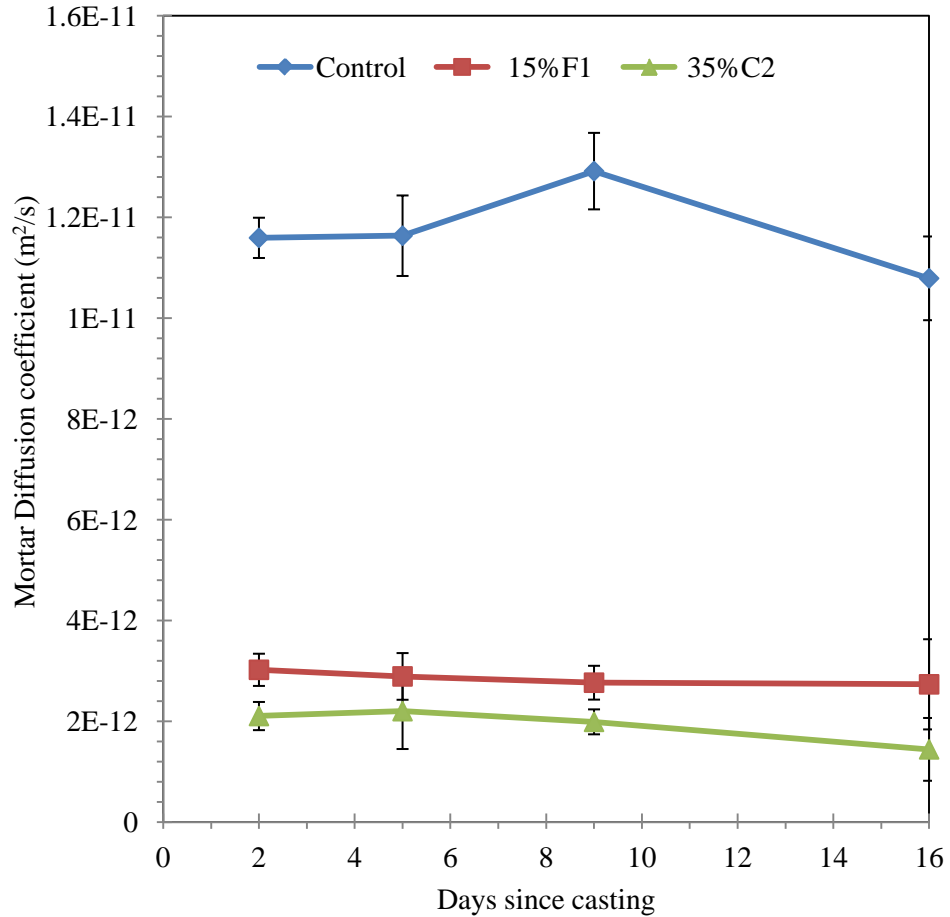
Figure 2-4: Ion diffusion coefficient of the control (100% PC), 15% F1 and 35% C2 mortars

2.5.4   Significance of alkali diffusion versus binding

It was observed in Figure 2-3(a) that fly ash mortars have a smaller concentration of OH$^-$ ions in their pore solution, which helps reduce the magnitude of ASR. Yet, it is not clear to what extent this reduction in [OH$^-$] is due to the lower ion diffusivity of mortars versus the mortars' improved alkali binding capacity. The numerical modeling results provided in Figure 2-5 are aimed at addressing this question. The figure shows the simulated [OH$^-$] profiles as a result of the penetration and binding of NaOH during the ASTM C1567 test. Here, the triangles represent the control (100% PC) mortar, where the OH$^-$ front has reached the centerline of the specimen (position = 12.5 mm) within 14 days of NaOH bath exposure. Larger [OH$^-$] would be anticipated at the specimen's interior had a more realistic 2D model been used, or if the model accounted for the effect of cracking on increasing the mortar diffusion coefficient.   SEM imaging confirmed the presence of ASR gel across the mortar's cross section, with higher severity of ASR attack at the specimen's surface.
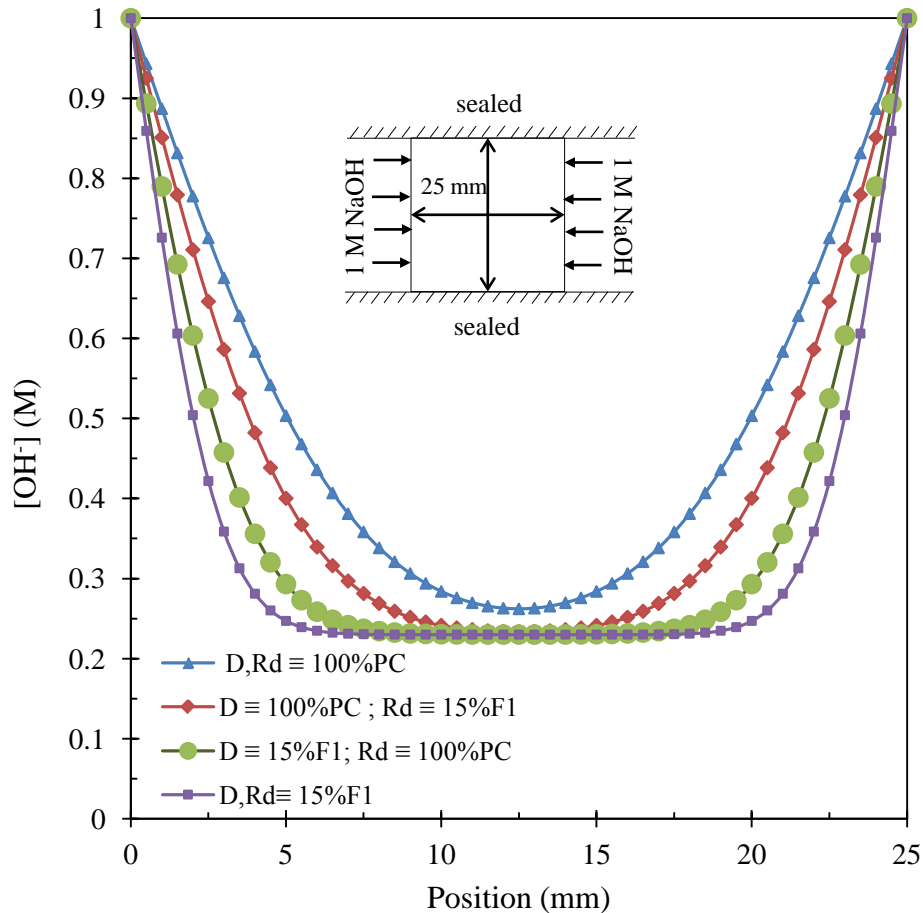
Figure 2-4: Simulation results showing the OH⁻ concentrations at the conclusion of ASTM C1567 testing for different diffusion and binding coefficients

The squares in Figure 2-5 show the simulated [OH⁻] profile corresponding to 15% F1 mortar. This mortar shows lower [OH⁻] due to a combination of lower ion diffusivity and higher C-S-H binding capacity. In comparison with the 100% PC mortar, the NaOH penetration depth was limited to approximately 5 mm from the surface, which accounts for ~60% of the specimen's cross sectional area. SEM results confirm the absence of ASR gel in this mortar, except within a few millimeters from the surface.

To evaluate the contributions of alkali binding versus ion diffusion on [OH⁻] profiles, two hypothetical mortars were simulated. The first mortar (shown as diamonds in Figure 2-5) had the same ion diffusivity as the 100% PC mortar but had a higher alkali binding capacity similar to 15% F1 mortar. The second mortar (shown as circles in Figure 2-5) had the same alkali binding capacity as the 100% PC mortar but had lower ion diffusivity similar to 15% F1 mortar. By comparison, it is evident that the effect of reduced ion diffusivity is more significant than the effect of improved alkali binding in reducing [OH⁻]. Overall, both mechanisms delay the penetration of NaOH which favors lesser ASR.

2.5.5   Tensile and compressive strength
The results of the tensile and compressive strength measurements of the mortars after 3 days submersion in NaOH solution are shown in Figure 2-6. The results are normalized by dividing by corresponding strengths of the control (100%PC) mortar. Commonly, it is assumed that replacing Portland cement with fly ash results in a reduction in the early-age strength (Pandey and Sharma 2000). In the environment of the ASTM C1567 test, however, it was observed that mortars containing fly ash showed a 15% to 38% increase in tensile strength compared to the 100% PC mixture. Improvement in

the compressive strength can be as high as 54%. Such strength improvements could be due to reduced pore size (i.e., flaw size) in fly ash mortars as reported in (Shafaatian 2012). The results of thermo-gravimetric analysis (TGA) and porosity measurements (not included here) show continuous consumption of portlandite and reduction of porosity with age in all fly ash mortars, which contributes to higher strengths.
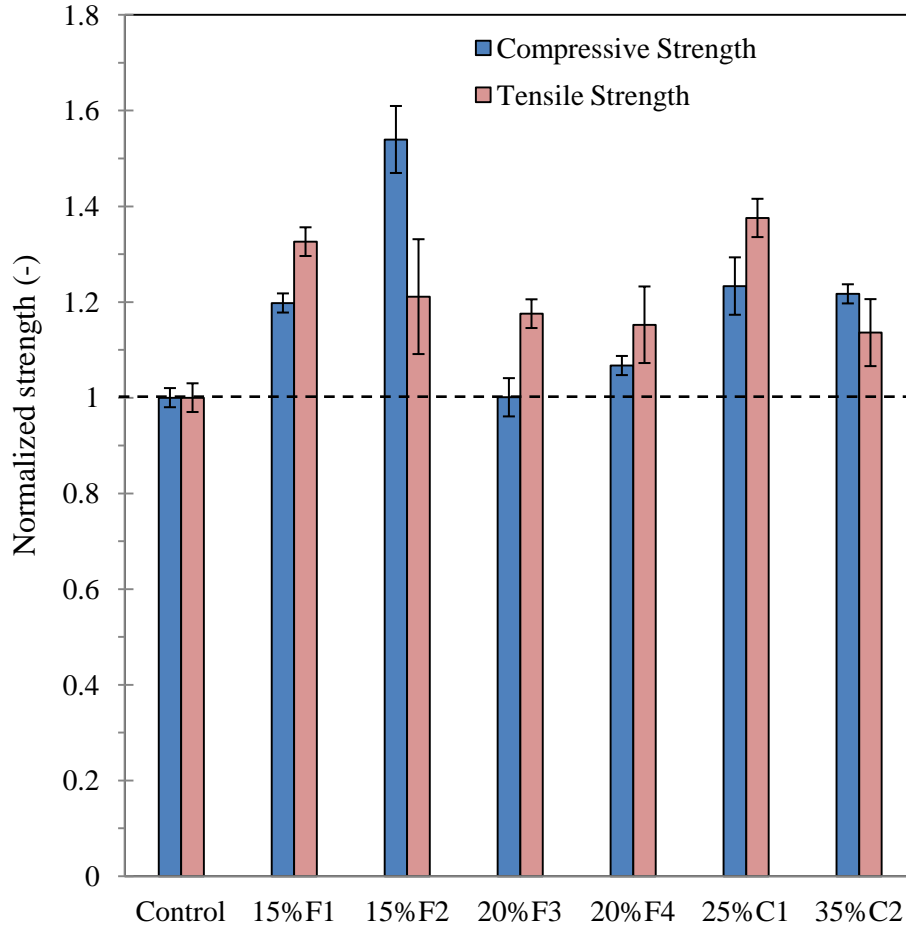

Figure 2-6: Normalized (to the control mortar) tensile and compressive strengths of mortars 3 days after exposure to 1M NaOH solution

An increase in the tensile strength of mortars in the ASTM C1567 test has two benefits. First, it prevents or delays the formation of cracks. Cracking provides immediate access of the NaOH solution to the interior of the specimen, which significantly accelerates ASR. Second, by delaying ASR, fly ash provides additional time to allow the hydration of the binder to proceed, which results in a denser and less permeable paste matrix. This can further mitigate alkali transport, formation and swelling of the gel, and cracking.

It should be noted that the increase in the early-age tensile strength of fly ash mortars may be an artifact of the ASTM C1567 test, which exposes specimens to high temperatures and alkalinities. Such an environment significantly promotes the pozzolanic reactions of fly ash. In real-life service exposures, the pozzolanic reaction of fly ash may result in higher tensile strengths only after a long term.
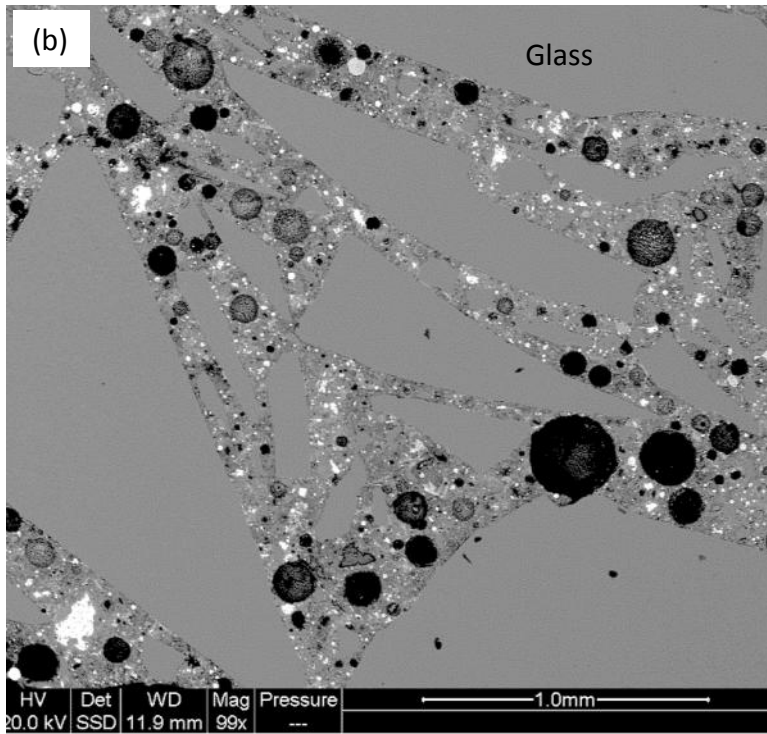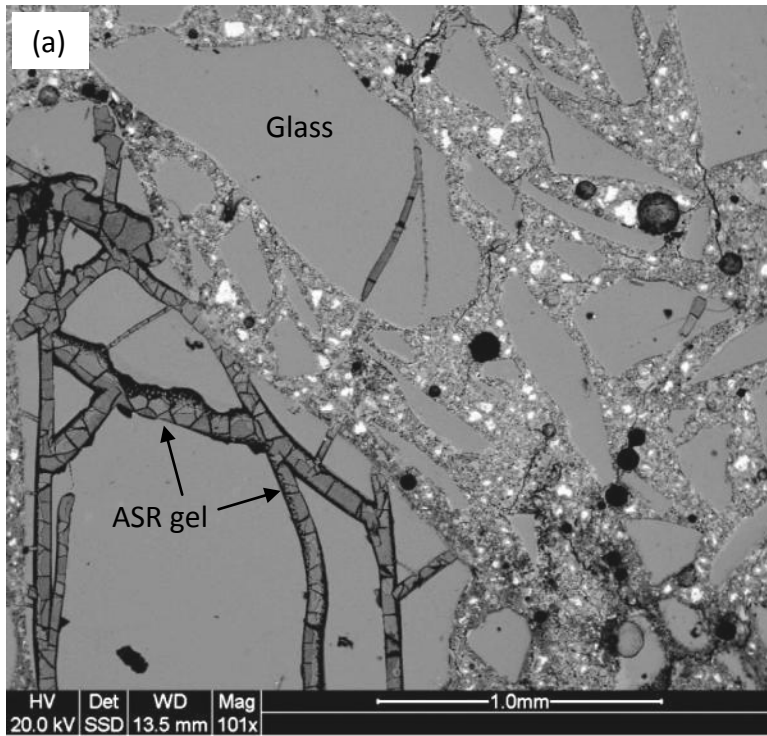
Figure 2-7: SEM micrographs of (a) control mortar, and (b) 15%F1 mortar at end of ASTM C1567 test

2.5.6   Microstructural analysis (SEM/EDS)

SEM/EDS imaging was performed to answer two main questions. First, does ASR gel form in large quantities in fly ash mortars? Second, does the presence of fly ash alter the composition of ASR gel and

as such, change its viscosity and swelling pressure, as suggested by Monteiro et al. (1997) and Bonakdar et al. (2010). Previous research by Bleszynski and Thomas (1998) on ASTM C1567 prisms containing reactive flint showed that significant dissolution of aggregates and formation of gel could occur in mortars containing fly ash. However, probably due to its low viscosity, this ASR gel could flow freely through the cement paste matrix without exerting large stresses and cracking.

Figures 2-7(a) and (b) show SEM images of the 100% PC and 15% F1 mortars at the conclusion of the ASTM C1567 test. While the control specimen was severely distressed by ASR, only minor traces of ASR gel were detected in the fly ash mortar. Other SEM images (not included) revealed that ASR was more severe at the perimeter versus the interior of mortar prisms, which is in agreement with the alkali transport mechanism driving the ASR. A summary of the EDS compositional analysis of the ASR gel from the control and fly ash mortars is presented in Table 2-2. The results show that the gel compositions were approximately similar; no significant differences on the Ca/Si or Ca/Na between the control and fly ash mortars were detected. This could mean that ASR gel has similar properties in all mortars. It is the massive volume of gel produced in the control mortar that leads to its deterioration, in comparison with small traces of gel in fly ash mortars. In addition, it was found that although the volume of gel formed increased with time in all mortars, there was only a slight variation in the gel composition based on EDS analysis between 7 and 14 days NaOH exposure. Also, variations in the gel composition from the perimeter to the interior of 100% PC mortar prisms were small.

Table 2-2: Average atomic composition (wt.%) of ASR gel measured by EDS

		Na	Ca	Si	K	Al	Mg	Ca/Si	Ca/Na
at 7 days	Control	7.76	4.91	24.81	1.29	0.64	0.37	0.2	0.63
	15%F1	9.04	5.33	24.37	1.66	1.56	1.44	0.22	0.59
	35%C2	8.95	5.23	24.49	2	1.19	-	0.21	0.58
at 14 days	Control	10.63	6.73	22.39	0.31	0.77	0.36	0.3	0.63
	15%F1	7.24	5.5	24.89	0.64	0.73	0.37	0.22	0.76
	35%C2	9.28	5.86	23.42	1.02	0.65	0.37	0.25	0.63

2.5.7 Aggregate dissolution rate

To evaluate the dissolution rate of glass aggregates and the potential benefits of fly ash, a glass corrosion experiment was performed in which the dissolution (i.e., mass loss) of soda-lime glass slides exposed to a constant volume (V=340 ml) of 1 M NaOH solution was monitored over time. Each corrosion cell contained two glass slides with a total surface area of SA=79×10^{-4}m^2. Duplicate experiments were performed in the absence of fly ash or by adding 10 g or 20 g of F1 fly ash (specific surface area = 0.2624 m^2/g) to the system.

The results are presented in Figure 2-8. The rate of mass loss from slides is higher in the system without fly ash. At 14 days, the mass loss of slides was 48% or 62% lower when 10 g or 20 g of fly ash was present. This is due to a drastic increase in the silicate surface area to solution volume ratio (SA/V) as a result of the silicate area provided by the fly ash (note that fly ash is mainly a silicate glass that also contains some crystalline silicate phases). While the solution volume remained at V=340 ml, the silicate surface area increased to SA=2.63 m^2 or SA=5.26 m^2 for 10 g or 20 g fly ash addition. As a result, the concentration of OH$^-$ ions (which are responsible for dissolving both glass slides and fly ash) decreased significantly per unit silicate surface area. For 340 ml 1 M NaOH solution, the OH$^-$ concentration per unit silicate surface area was 43,038 mM/m^2 when no fly ash is present. This value droppped to 129.3 or 64.6 mM/m^2 when 10 g or 20 g of F1 fly ash was added. The rate of glass slide corrosion increased with time, mainly due to an increase in the pH of the solution as a result of the ion exchange reaction presented by equation (3). Starting from the initial [OH$^-$]=1000 mM, the [OH$^-$] in the solution reached 1060 mM at 14 days when no fly ash was present. For the system with 10 g fly ash, [OH$^-$]=1150 mM at 14 days.
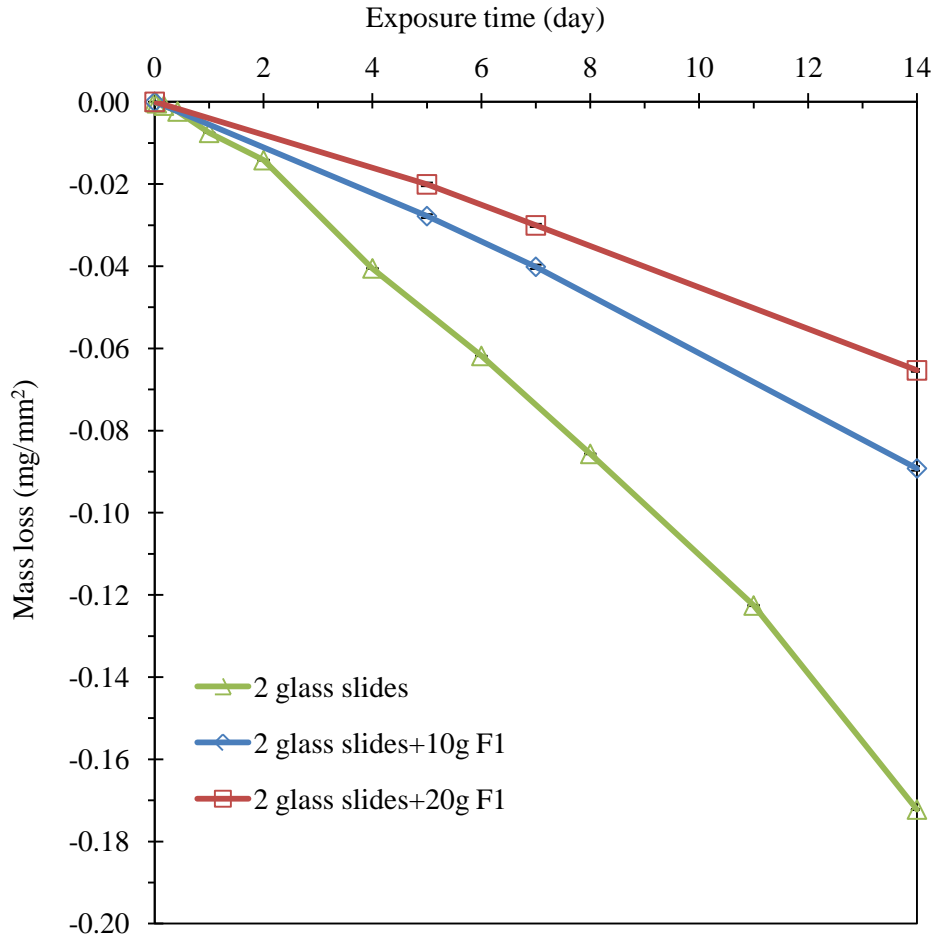
Figure 2-8: Mass loss of glass slides in 1M NaOH solution at 80ºC in the presence or absence of fly ash

The results presented in Figure 2-8 suggest a new mechanism by which supplementary cementitious materials (SCMs) can mitigate ASR. By increasing the accessible silicate surface area, the SCM reduces the effective concentration of OH⁻ at the surface of aggregates and as such, reduces the aggregate dissolution rate. Even if no subsequent pozzolanic reaction occurs (e.g., due to a local absence of portlandite), the mere presence of SCM increases the accessible silicate surface area and reduces the aggregate dissolution rate. To our knowledge, this mechanism has not been previously discussed in the ASR literature.

2.6   Conclusions
The results of this study suggest that fly ash can effectively mitigate ASR in ASTM C1567 testing through the following mechanisms:

- Fly ash reduces the alkalinity ([OH⁻]) of pore solution by significantly reducing the ion diffusion coefficient of mortars. A diffusivity reduction by a factor of 4 to 7 was recorded, as early as 48 hours after casting, when sufficient dosage of fly ash replaced Portland cement. As such, the external NaOH penetrates more slowly into fly ash mortars, resulting in a lower pore fluid alkalinity and significantly slower ASR.

- Fly ash reduces the alkalinity ([OH⁻]) of pore solution through alkali binding. Fly ash reduces the calcium to silica ratio (C/S) of C-S-H gel, which in turn improves its alkali binding capacity. In

addition, more C-S-H is produced by pozzolanic reactions. As such, a considerable fraction of the penetrated NaOH is removed from the pore solution. The results of a simple numerical model suggested that the contribution of transport reduction is more significant than the effect of improved alkali binding.

- Fly ash increases the tensile strength of mortars and prevents or delays the onset of cracking. This also prevents an accelerated transport of NaOH through cracks to the interior of mortar specimens.

- Fly ash can reduce the dissolution rate of siliceous aggregates even when the pH of pore solution is maintained constant (e.g., near the perimeter of mortar prisms that are exposed to external NaOH bath). Fly ash provides a large silicate surface area that is accessible to the corrosive OH^- ions. As such, the concentration of OH^- per unit surface area of silicate is markedly reduced. In other words, for a unit volume of pore solution at a given pH, a significant fraction of hydroxyl ions are involved in dissolving fly ash instead of attacking the reactive aggregates.

The results of this work also suggest that alkali dilution and modifying ASR gel composition are not major contributors to the mitigation of ASR by fly ash in ASTM C1567 testing.

References
- A. Akhavan, F. Rajabipour, Evaluating ion diffusivity of cracked cement paste using electrical impedance spectroscopy, Submitted to Materials and Structures, 2012
- ASTM C150/C150M-11, Standard Specification for Portland Cement, 2011, American Society for Testing and Materials, West Conshohocken, Pennsylvania, USA
- ASTM C305-06, Standard Practice for Mechanical Mixing of Hydraulic Cement Pastes and Mortars of Plastic Consistency, 2006, American Society for Testing and Materials, West Conshohocken, Pennsylvania, USA
- ASTM C311-07, Standard Test Method for Sampling and Testing Fly Ash or Natural Pozzolans for Use in Portland-Cement Concrete, 2007, American Society for Testing and Materials, West Conshohocken, Pennsylvania, USA
- ASTM C618-08a, Standard Specification for Coal Fly Ash and Raw or Calcined Natural Pozzolan for Use in Concrete, 2008, American Society for Testing and Materials, West Conshohocken, Pennsylvania, USA
- ASTM C1293-08b, Standard Test Method for Determination of Length Change of Concrete Due to Alkali-Silica Reaction, 2008, American Society for Testing and Materials, West Conshohocken, Pennsylvania, USA
- ASTM C1567-07, Standard Test Method for Determining the Potential Alkali-Silica Reactivity of Combinations of Cementitious Materials and Aggregates (Accelerated Mortar-Bar Method), 2007, American Society for Testing and Materials, West Conshohocken, Pennsylvania, USA
- R.F. Bleszynski, M.D.A. Thomas, Microstructural studies of alkali-silica reaction in fly ash concrete immersed in alkaline solutions, Advanced Cement Based Materials, 1998, 7(2), 66-78
- A. Bonakdar, B. Mobasher, S.K. Dey and D.M. Roy, Correlation of reaction products and expansion potential in alkali-silica reaction for blended cement materials, ACI Materials Journal, 2010, 107(4), 380-386
- I. Canham, C.L. Page and P.J. Nixon, Aspects of the pore solution chemistry of blended cements related to the control of alkali silica reaction, Cement and Concrete Research, 1987, 17(5), 839-844
- B.J. Christensen, T. Coverdale, R. A. Olson, S. J. Ford, E. J. Garboczi, H. M. Jennings, T. O. Mason, Impedance Spectroscopy of Hydrating Cement-Based Materials: Measurement, Interpretation, and Application, Journal of the American Ceramic Society 1994, 77(1), pp. 2789–2804
- D.E. Clark, E.L. Yen-Bower, Corrosion of glass surfaces, Surface Science, 1980, 100, pp. 53-70
- CRC Handbook of chemistry and physics, 90th Ed., CRC Press, Boca Raton, Florida, 2010
- J. Duchesne and M.A. Bérubé, The effectiveness of supplementary cementing materials in suppressing expansion due to ASR; II: Pore solution chemistry, Cement and Concrete Research, 1994, 24(8), 1579-1581
- D.W. Hobbs, Alkali-Silica Reaction in Concrete, Thomas Telford, London. 1988

- S.Y. Hong, F.P. Glasser, Alkali binding in cement pastes: Part I. The C-S-H phase, Cement and Concrete Research, 1999, 29(12), 1893-1903
- S.Y. Hong, F.P. Glasser, Alkali sorption by C-S-H and C-A-S-H gels: Part II. Role of alumina, Cement and Concrete Research, 2002, 32(7), 1101-1111
- Y. Li, Y. Chen, J. Wei, X. He, H. Zhang, W. Zhang, A study on the relationship between porosity of the cement paste with mineral additives and compressive strength of mortar based on this paste fla, Cement and Concrete Research, 2006, 36(9), pp. 1740-1743
- B. Lothenbach, K.Scrivener, R.D. Hooton, Supplementary cementitious materials, Cement and Concrete Research, 2011, 41, 217–229
- L.J. Malvar, L.R. Lenke, Efficiency of fly ash in mitigating alkali-silica reaction based on chemical composition, ACI Materials Journal, 2006, 103(5), 319-326
- S. Mindess, J.F. Young, D. Darwin, Concrete, 2nd Ed., 2003, Pearson Education, Upper Saddle River, New Jersey, USA
- P.J.M. Monteiro, K. Wang, G. Sposito, M.C. dos Santos and W.P. de Andrade, Influence of mineral admixtures on the alkali-aggregate reaction, Cement and Concrete Research, 1997, 27(12), 1899-1909
- S.P Pandey, R.L Sharma, The influence of mineral additives on the strength and porosity of OPC mortar, Cement and Concrete Research, 2000, 30(1), pp. 19-23
- F. Rajabipour, Insitu electrical sensing and material health monitoring in concrete structures, Ph.D. Dissertation, Purdue University, West Lafayette, Indiana, Dec. 2006, 193pp
- F. Rajabipour, G. Sant and J. Weiss, Interactions between shrinkage reducing admixtures (SRA) and cement paste's pore solution, Cement and Concrete Research, 2008, 38(5), pp. 606–615
- P.L. Rayment, The effect of pulverised-fuel ash on the c/s molar ratio and alkali content of calcium silicate hydrates in cement, Cement and Concrete Research, 1982, 12(2), pp. 133-140
- S.M.H. Shafaatian, H. Maraghechi, F. Rajabipour, Assessing the role of ion transport in mitigation of ASR by fly ash in accelerated mortar bar test, Submitted to ASCE Journal of Materials in Civil Engineering, 2012
- M.H. Shehata, M.D.A. Thomas, The effect of fly ash composition on the expansion of concrete due to alkali–silica reaction, Cement and Concrete Research, 2000, 30(7), 1063-1072
- M.H. Shehata, M.D.A.Thomas, Alkali release characteristics of blended cements, Cement and Concrete Research, 2006, 36(6), 1166-1175
- L.J. Struble, S. Diamond, Swelling properties of synthetic alkali silica gels, Journal of the American Ceramic Society, 1981, 64(11), 652–655
- R.N. Swamy, The Alkali-Silica Reaction in Concrete, Routledge, 1992
- M.D.A. Thomas, The effect of supplementary cementing materials on alkali-silica reaction: A review, Cement and Concrete Research, 2011, 41, 209-216

CHAPTER 3:
PROPORTIONING AND EVALUATION OF GLASSCRETE MIXTURES

3.1.   Introduction

The main focus of this chapter is proportioning and testing concrete mixtures containing recycled glass as 100% replacement of natural sand (i.e., fine aggregates). Such mixtures will be termed "Glasscrete." Mix proportioning was performed in accordance with ACI 211.1 to achieve a target slump (1.5 or 5 inches), air content (3%), and 28-day compressive strength (4000 or 5000 psi). Trial batches were prepared, tested, and concrete proportions (including the dosages of super-plasticizer and air entraining admixture) were adjusted to achieve target slump, air content, and strength. In addition, several hardened properties of glasscrete were measured and compared with those of concrete made with natural sand. Comparisons were made based on a comparable 28-day compressive strength or a comparable w/cm.

Table 3-1 provides a list of mixtures prepared and tested in this chapter. The mixture ID starts with a letter N (representing natural sand) or G (representing glass sand). This is followed by a number that represents the design 28-day compressive strength of each mixture in ksi. Next, the target slump is provided (1.5 or 5 inches). The only exception to this naming protocol is the last mixture, which is made with natural sand, has a w/cm=0.48, and has a target slump of 5 inches.

Table 3-1: Naming system for mixtures.

Mixture	Design Strength (ksi)	Design Slump	Fine Aggregate	Potential Applications
N5,5.0"	5000	5.0"	Natural Sand	Building Frames and Bridge Decks
G5,5.0"	5000	5.0"	Glass Sand	Building Frames and Bridge Decks
N4,5.0"	4000	5.0"	Natural Sand	Building Frames and Bridge Decks
G4,5.0"	4000	5.0"	Glass Sand	Building Frames and Bridge Decks
N4,1.5"	4000	1.5"	Natural Sand	Pavements or Slip-Form Applications
G4,1.5"	4000	1.5"	Glass Sand	Pavements or Slip-Form Applications
N0.48,5.0"	---	1.5"	Natural Sand	Building Frames and Bridge Decks

The bulk of the research compared the properties of glasscrete and natural sand concretes at similar design compressive strengths. For example, a comparison between mixtures N5,5.0" and G5,5.0" provides material designers with an understanding of the hardened properties of glasscrete when it is designed to achieve a required 28-day compressive strength of 5000 psi. This is a typically replicated procedure that allows for a fundamental understanding of the concrete's composition versus strength that can then be expanded upon to improve the material's quality (Popovics 1990). A significant outcome of this step is the development of mixture proportioning charts relating w/cm of glasscrete mixtures to their compressive strength. It has been shown that the use of recycled glass sand may reduce the compressive strength of concrete (Rajabipour et al. 2009); and to compensate for this effect, the w/cm of the mixture could be reduced. However, no specifications currently exist to show what w/cm must be chosen by materials designers to achieve a target compressive strength. An example of such a w/cm-strength chart is provided in ACI211.1 and the PCA design handbook for concrete with natural aggregates (Kosmatka and Wilson 2011), and is shown in Figure 3-1.
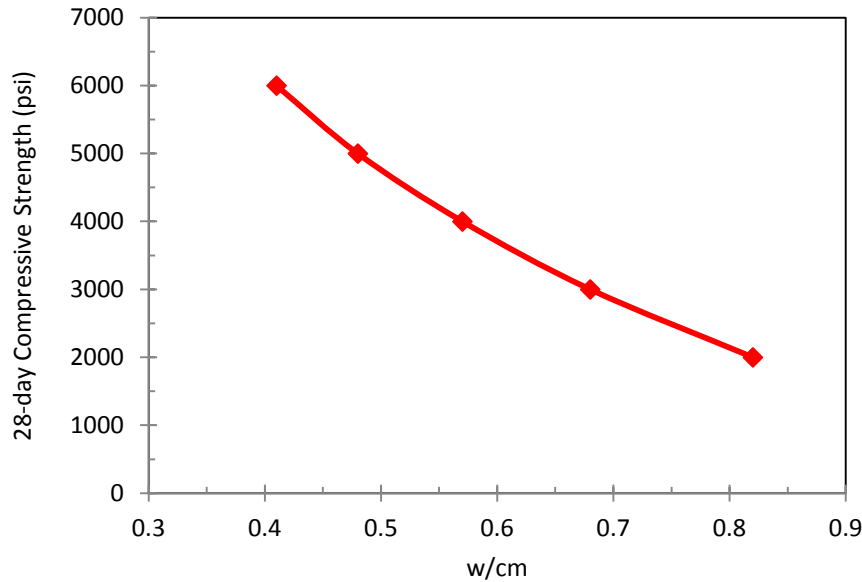
Figure 3-1: ACI 211.1 correlation between the 28-day compressive strength of a non-air-entrained Portland cement concrete mixture and its water to cementitious materials ratio (w/cm)

Another set of comparisons was made between the properties of glasscrete and natural sand concrete mixtures that have the same w/cm ratio. The objective was to determine the effect of use of glass sand on the hardened properties of concrete when the cement paste composition and the volume fraction of cement paste remain constant. In both sets of comparisons, the following fresh and hardened properties of concrete were examined:

- Slump: according to ASTM C143
- Plastic air content by pressure method: according to ASTM C231
- Time of setting of mortar: according to ASTM C403
- Compressive strength: according to ASTM C39
- Linear coefficient of thermal expansion of mortar: according to ASTM C531
- Abrasion resistance: according to ASTM C944
- Rapid chloride permeability: according to ASTM C1202
- Water sorptivity: according to ASTM C1585

In all concrete mixtures, 20% class F fly ash (F2 fly ash from chapter 2 was used to mitigate the potential for alkali-silica reaction. Given that these concrete mixtures were primarily developed for application in the State of Hawaii, a target air content of 3.0% was used, representing a mild freezing and thawing exposure. In addition, concrete was assumed not to be exposed to deicers and other aggressive substances that may induce corrosion or sulfate attack. Alternatively, for concretes that may be exposed to such deleterious conditions, the material designer should make adjustments in the mixture proportions (e.g., w/cm, air content) to minimize the risk of damage and ensure long-term durability.

3.2. Materials
The following sections will discuss the constituents that were used in proportioning the concrete mixtures. The basic concrete constituents are coarse aggregate, fine aggregate, water, air, cement, and fly ash. Plasticizers and air-entraining admixtures were also used throughout this study. The coarse aggregate, water, cement, and fly ash did not differ in properties across the natural sand concrete and glasscrete mixtures. However, the fine aggregate's properties changed due to glass being used as a 100% fine aggregate replacement for glasscrete systems.

3.2.1. Portland cement and fly ash

ASTM C150 Type I Portland cement was used throughout this work. The cement was procured from a supplier in Nazereth, PA. ASTM C618 class F fly ash was used with a specific gravity of 2.4 to mitigate ASR. The oxide composition of cement and F2 fly ash are provided in Table 2-1.

3.2.2. Chemical admixtures

Both a super-plasticizer and an air-entraining admixture were used during this study. The super-plasticizer was Glenium 7710, manufactured by BASF, and was used to achieve proper consistency (target slump of 1.5 or 5 inches) for different mixtures. The air-entraining admixture was MB-AE 90, also manufactured by BASF. The air entrainer was used to obtain the target plastic air content of 3.0%.

3.2.3. Coarse aggregates

The coarse aggregate was a locally available crushed limestone and had a gradation in accordance with ASTM C33 #57 aggregate. The maximum size aggregate (MSA) was 1.0" and all aggregate smaller than the #4 sieve were expelled via a wet sieving procedure. The aggregate was batched at oven dried conditions (mixed at room temperature) and used both for glasscrete and natural sand concrete mixtures. The aggregate properties were as follows:
- Dry-Rodded Unit Weight (DRUW): 95.51 lb/ft^3
- Oven-Dried Specific Gravity: 2.80
- Absorption Capacity: 0.60%

3.2.4. Natural sand

Natural river sand (as seen juxtaposed to glass sand in Figure 3-2) adhered to ASTM C33 for use as a fine aggregate in concrete. The fineness modulus for the sand was measured as 2.93. The aggregate size distribution is provided in Table 3-2. The sand was batched at oven-dried conditions (mixed at room temperature) throughout the study. The natural sand properties were as follows:
- Oven-Dried Specific Gravity: 2.60
- Absorption Capacity: 0.96%

Figure 3-2: 3000 revolution glass sand (left) and natural river sand (right) as used in concrete production

Table 3-2: Sieve analysis for natural sand

Sieve Size	Cumulative % Retained
3/8"	0
#4	2
#8	22
#16	38
#30	55
#50	81
#100	95
FM (ASTM C 125)	2.93

3.2.5. Glass sand

Coarse crushed glass cullet was procured from a local recycling company that provided super-sacks of clear glass cullet and mixed color glass cullet (mainly green and amber). A mixture of 2 lb of mixed color cullet to 1 lb of clear cullet was used in glasscrete mixture. The following process was followed to produce fine glass aggregates. Special attention was paid to ensure that glass sand had a particle size distribution and fineness modulus as close as possible to the natural sand (Table 3-2).

1. Obtain recycled glass cullet ranging in size from 1/16 inch to 1 inch.
2. Wash glass cullet thoroughly using a wet sieve approach to expel deleterious materials such as paper and organics (similar to the approach of Polley et al. (1998)).
3. Place glass cullet in stainless steel trays inside oven and heat until all water has evaporated.
4. Remove oven dried glass cullet and allow it to cool to room temperature.
5. Place approximately 20 lb of glass cullet in a standard Los Angeles (LA) Abrasion Machine (Figure 3-3).
6. Two different revolution quantities were used to obtain glass sand, as described below:
   (a) Rotate 20 lb of glass cullet for 1000 revolutions. Remove all glass aggregate from the LA Abrasion Machine. Expel all glass particles retained on sieve #4. The final product is shown in Figure 3-4.
   (b) Rotate a different 20-lb batch of glass cullet for 3000 revolutions. Remove all glass particles retained on sieve #4 and passing sieve #100. A wet sieve procedure is employed in order to remove aggregate passing the #100 sieve. After the process is complete, oven dry the aggregate. The final product is shown in Figure 3-2.
7. Allow separate containers to store the aggregate of the 1000 revolutions and the aggregate of the 3000 revolutions.

Figure 3-3: LA Abrasion Machine used to crush glass cullet to sand size

Figure 3-4: 1000 revolution glass sand used in production of concrete mixtures

A trial and error approach was used to fine tune details of the glass sand preparation procedure. The resulting data showed that by blending the 1000 revolution glass aggregate and 3000 revolution glass aggregate on a 50/50 basis, the aggregate size distribution comparable to the natural sand (Table 3-2) can be obtained. The fineness modulus of glass sand produced by this blending is similar to the natural sand and is approximately 3.00. Table 3-3 shows the aggregate size distribution of recycled glass sand measured at several times throughout the research. The fineness modulus (FM) is defined by ASTM C125 as the sum of the cumulative percentages retained on the standard sieves between the numbers #4 and #100 divided by 100. According to ASTM C33, the FM may fluctuate within 0.20 for a given concrete mixture design. Since the FMs of glass sand fluctuated between 2.98 and 3.08 and the FM of natural sand at 2.93 are all within 0.20 of each other, the FM of 3.00 was used in the design of concrete mixtures throughout this study.

The aggregate was batched at oven-dried conditions (mixed at room temperature). Other properties of the glass sand were as follows:
  – Oven Dried Specific Gravity: 2.53
  – Absorption Capacity: 0.00%

3.3. Experimental Methods
3.3.1. Mixture proportioning
A total of seven concrete mixtures were proportioned in this work including 3 glasscrete and 4 natural sand concrete mixtures. The naming protocol and the target values for slump and compressive strength of each mixture are provided in Table 3-1. Proportioning was performed according to ACI 211.1. Trial batches were prepared and the slump, air content, and 7-day compressive strength of the mixtures were measured. The proportions were adjusted accordingly to achieve target design values by modifying the w/cm and the dosages of the super-plasticizer and air-entraining admixtures. The final proportions for each mixture are provided in Table 3-4.

In the following, a brief description of some of the experimental methods is provided. Slump and plastic air content were measured according to ASTM C143 and C231, respectively. For the measurement of the time of setting and the coefficient of thermal expansion, corresponding mortar mixtures were tested instead of concrete. Mortars were proportioned by removing the coarse aggregate from concrete proportions provided in Table 3-4. The final proportions of mortar mixtures are provided in Table 3-5.

Table 3-3: Sieve analysis for fine glass sand

Sieve Size	5/24/2011			6/7/2011		
	Cumulative % Retained (1000 Revs)	Cumulative % Retained (3000 Revs)	Overall % Retained	Cumulative % Retained (1000 Revs)	Cumulative % Retained (3000 Revs)	Overall % Retained
(3/8) in	0	0	0	0	0	0
#4	0	0	0	0	0	0
#8	21	15	18	24	14	19
#16	46	40	43	44	40	42
#30	66	64	65	64	64	64
#50	82	85	83.5	84	88	86
#100	93	100	96.5	92	100	96
FM	3.08	3.04	3.06	3.08	3.06	3.07

Sieve Size	9/20/2011			12/12/2011		
	Cumulative % Retained (1000 Revs)	Cumulative % Retained (3000 Revs)	Overall % Retained	Cumulative % Retained (1000 Revs)	Cumulative % Retained (3000 Revs)	Overall % Retained
(3/8) in	0	0	0	0	0	0
#4	0	0	0	0	0	0
#8	25	9	17	18	10	14
#16	50	35	42.5	41	38	39.5
#30	67	62	64.5	69	59	64
#50	86	85	85.5	84	80	82
#100	97	100	98.5	96	100	98
FM	3.25	2.91	3.08	3.08	2.87	2.98

3.3.2.   Time of setting of mortar by penetration resistance (ASTM C403)

The initial time of setting is defined as the time when mortar loses its plastic consistency. The final set time is defined as the time when mortar can begin to sustain load (Hewlett 1998). These setting times can be measured according to ASTM C403 using a mortar penetrometer (Figure 3-5a). After mixing (per ASTM C305), the fresh mortar mixture was placed into a 6x6 inch diameter x height plastic cylinder. The cylinder was filled in three layers and compacted using a vibrating table. The cylinder was placed in a moist curing room for the duration of the testing and was only removed to take measurements. Three separate specimens were tested for each mixture.

Measurements were performed using a spring-reaction penetrometer (Figure 3-5a). This device allows for a needle with a bearing diameter of ¼ inch to be thrust into the setting mortar (Figure 3-5b) in order to attain a pressure/resistance reading. The needle is forced to penetrate 1 inch into the mortar. Upon penetrating the mortar, the spring-reaction provides a force reading in pounds, required to penetrate the needle into the mortar by 1 inch. This force reading is divided by the penetration area (0.049 in^2) to find the penetration resistance (stress) in psi. Initial setting time is defined as the time when the penetration resistance is equal to 500 psi and the final setting time occurs when the penetration resistance is equal to 4000 psi.

Table 3-4: Proportions of final concrete mixtures (aggregates weight provided in oven-dried condition)

	N5,5.0"	G5,5.0"	N4,1,5"	G4,1,5"	N4,5.0"	G4,5.0"	N0.48,5.0"
Design 28-day f'c (lb/in^2)	5000	5000	4000	4000	4000	4000	---
Design Slump (in)	5.0"	5.0"	1.5"	1.5"	5.0"	5.0"	5.0"
Design Air Content (%)	3.0	3.0	3.0	3.0	3.0	3.0	3.0
Measure 28-day f'c (lb/in^2)	5420	5060	4040	4240	4200	4070	4750
Measured Slump (in)	4.5-5.5	4.5-5.5	1.5-1.75	1.25-1.50	4.5-5.5	4.5-5.5	4.5-5.5
Measured Air Content (%)	2.0-4.0	2.0-4.0	2.0-4.0	2.0-4.0	2.0-4.0	2.0-4.0	2.0-4.0
Cement (lb/yd^3)	539.1	590.5	421.0	450	424.6	504.2	504.2
Fly Ash (lb/yd^3)	134.8	147.6	105.3	112.5	106.1	126.0	126.0
Water* (lb/yd^3)	310	310	300	270	302.5	302.5	302.5
Coarse Aggregate (lb/yd^3)	1676.2	1676.2	1676.2	1676.2	1676.2	1676.2	1676.2
Fine Aggregate (lb/yd^3)	1285.9	1193.8	1442.2	1446.4	1431.9	1305.8	1344
w/cm	0.46	0.42	0.57	0.48	0.57	0.48	0.48
Paste Content (%)	32.9	34.2	29.2	28.1	29.5	31.5	31.5

* Not including water absorption of aggregates

Table 3-5: Proportions of mortar mixtures (sand weight provided in oven-dried condition)

	N5,5.0"	G5,5.0"	N4,1,5"	G4,1,5"	N4,5.0"	G4,5.0"	N0.48,5.0"
Cement (lb)	539.1	590.5	421.0	450	424.6	504.2	504.2
Fly Ash (lb)	134.8	147.6	105.3	112.5	106.1	126.0	126.0
Water* (lb)	310	310	300	270	302.5	302.5	302.5
Fine Aggregate (lb)	1285.9	1193.8	1442.2	1446.4	1431.9	1305.8	1344
w/cm	0.46	0.42	0.57	0.48	0.57	0.48	0.48
Yield (yd^3)	0.61	0.61	0.61	0.61	0.61	0.61	0.61
Paste Content (%)	53.8	55.9	47.7	46.0	48.1	51.5	51.5

* Not including water absorption of aggregates

Figure 3-5: (a) Humboldt H/4133 spring-reaction device used for measurement of time of setting of mortar; (b) Mortar specimen after completion of setting time measurements

The time of setting clock begins at the moment water comes into contact with cementitious materials. The initial reading occurs 2 to 3 hours post contact, with subsequent readings occurring at 30-minute intervals. At least 6 penetrations are necessary to create a penetration resistance versus time curve that can be used to find the initial and final time of setting by interpolation. Also, one reading must be less than or equal to 500 psi and one reading must be greater than or equal to 4000 psi in order to properly capture the setting characteristics of the mortar mixture.

3.3.3.   Compressive strength (ASTM C39)
The unconfined compressive strength of concrete was measured using 4x8-inch cylinders. The cylinders were cast in three layers and compacted via 25 rods at each layer. All specimens were moist cured for the duration of their lifetime until moments before testing. The tops were smoothed with a diamond cut wet saw to provide an even surface for loading. The cylinders were tested for each mixture at 1, 3, 7, 28, and 90 days after casting. For each mixture and age, three duplicate cylinders were tested in accordance with ASTM C39. The cylinders were tested using a Boart Longyear model CM-625 with a CSI Model CS-100-2A Retrofit allowing for an instantaneous readout of the load imposed on the specimen. According to the standard, a rate of 35+/-7 (psi/sec) was applied to the cylinder. Both the load (lbf) and the stress (psi) were recorded.

3.3.4.   Coefficient of Thermal Expansion (ASTM C 531)

Thermal properties of concrete are important for the design of concrete structures when the structure is exposed to sustained high temperatures, used for thermal insulation, or used for fire protection (Mindess et al. 2003). In addition, the coefficient of thermal expansion (COTE) has a significant impact on the thermal cracking tendency of mass concrete as well as restrained concrete members at early ages (ACI 231). The coefficient of thermal expansion quantifies the thermal strain of concrete in response to a unit increase or decrease in the temperature. As concrete hydrates, it warms due to heat of hydration. Concrete often sets near its peak temperature. As the concrete cools to ambient temperature, it undergoes thermal contraction. Thermal contraction results in tensile stresses and the risk of cracking when the concrete is restrained (e.g. in pavements or bridge decks). A larger COTE results in a greater thermal contraction and a higher risk of cracking.

The coefficient of thermal expansion of concrete is dependent on the volume fraction of cement paste (COTE typically in the range 10~20 x10^{-6} /^{o}C), as aggregates generally show lower COTE (typically in the range 5~10 x10^{-6} /^{o}C) (Emanuel and Hulsey 1977, West 1994). Large differences in coefficients of thermal expansion between the aggregate and the paste may cause differential expansion in the mortar and therefore cause cracking in the specimen (Mindess et al. 2003). In addition, moisture content of concrete can significantly affect its COTE; thermal expansion is known to be the highest in the relative humidity (RH) range of 50~70% and lower for very dry or for saturated concrete (Bazant 1970, Zoldners 1971, Sellevold and Bjøntegaard 2006). This is due to the fact that change in temperature changes the internal RH of concrete, its moisture retention properties, as well as the surface tension of water. As such, the temperature change can cause hygrothermal shrinkage or swelling due to moisture loss or gain, and this is in addition to any volume changes due to thermal expansion or contraction of the solid skeleton (Grasley 2003). In addition to the moisture/RH, lower porosity of cement paste (achieved by lower w/cm and age) could reduce its COTE (Emanuel and Hulsey 1977).

In this work, the COTE was found for mortar mixtures at saturated condition. Mortar bars (1x1x10 inches according to ASTM C490) were used to focus on the fine aggregate's role on the COTE and limit the temperature gradients that could develop in larger prisms containing coarse aggregate. Mortars were mixed according to ASTM C 305 and cast in prism molds using a vibrating table. Embedded nickel studs were used to facilitate length measurements. The studs had a coefficient of thermal expansion of 7.2x10^{-06}/^{o}F, which was accounted for in the COTE calculations. Testing began after the specimens had been moist cured for 14 days. The results from four duplicate prisms were used and averaged to determine the COTE of each mixture in the saturated condition. The saturated specimens were heated from room temperature (23 ^{o}C or 73.4 ^{o}F) to a temperature of 80 ^{o}C (176 ^{o}F) while fully submerged in saturated lime-water. After at least 16 hours at 80 ^{o}C, the specimens' length was recorded using a Humboldt digital comparator model BG2600-16001. The temperature of the limewater bath was checked periodically using a thermometer. Mortar bars were removed from the 80 ^{o}C bath one by one and their length measured to the nearest 0.0001 inch. The specimens were then submerged back into the limewater bath and cooled to a temperature of 60 ^{o}C (140°F). After at least 16 hours at 60 ^{o}C, the specimens' length was recorded. This temperature cycle (60 ^{o}C to 80 ^{o}C and reverse) continued until the specimens reached constant lengths at both 60 ^{o}C and 80 ^{o}C.

3.3.5.   Abrasion Resistance (ASTM C 944)

Abrasion resistance is an important parameter to predict the wearing durability of concrete floors, pavements, and bridge decks. Abrasion is quantified as the repeated frictional rubbing (attrition) that is typically associated with pavements or industrial floors (Mindess et al. 2003). Abrasion resistance is therefore the ability of the concrete to resist this attrition. Aggregate-cement paste bond tends to have a significant impact on the abrasion resistance of concrete. The bond could be the weakest point and tend to be the fastest abrading part of concrete. The aggregate type and porosity (w/cm) of the binder also play a role in the abrasion resistance of concrete. If the w/cm is low enough, the cement paste can form a strong binder around the aggregates, which makes the abrasion resistance less dependent on the aggregate type (Mindess et al. 2003). The surface finishing is also important to the abrasion resistance of concrete (Mindess et al. 2003).

For the purposes of this test, disk specimens were cut from an interior section of a 6-inch-by-12-inch concrete cylinder as seen in Figure 3-6a. Three duplicate specimens were tested for each mixture. The concrete cylinder had been moist cured for 27 days. After moist curing, the concrete cylinder was cut and the disks were allowed to air-day for 24 hours. This was employed to limit the mass loss due to moisture loss during the test. Next, disk specimens were loaded onto a drill press and secured in place with a set of large clamps. These clamps hold the specimen in place while two rotating cutters are lowered on top of the specimen. These rotating cutters are free to spin on the concrete surface while carrying a vertical load of 44 lbf. The cutters are spinning at 200 revolutions per minute. The concrete specimens were abraded three separate times for 2-minute durations. The specimens' mass is determined before the initial abrasion and after each successive interval. The results report the overall mass loss as an indicator of the abrasion resistance of concrete. The test setup is shown in Figure 3-6b.
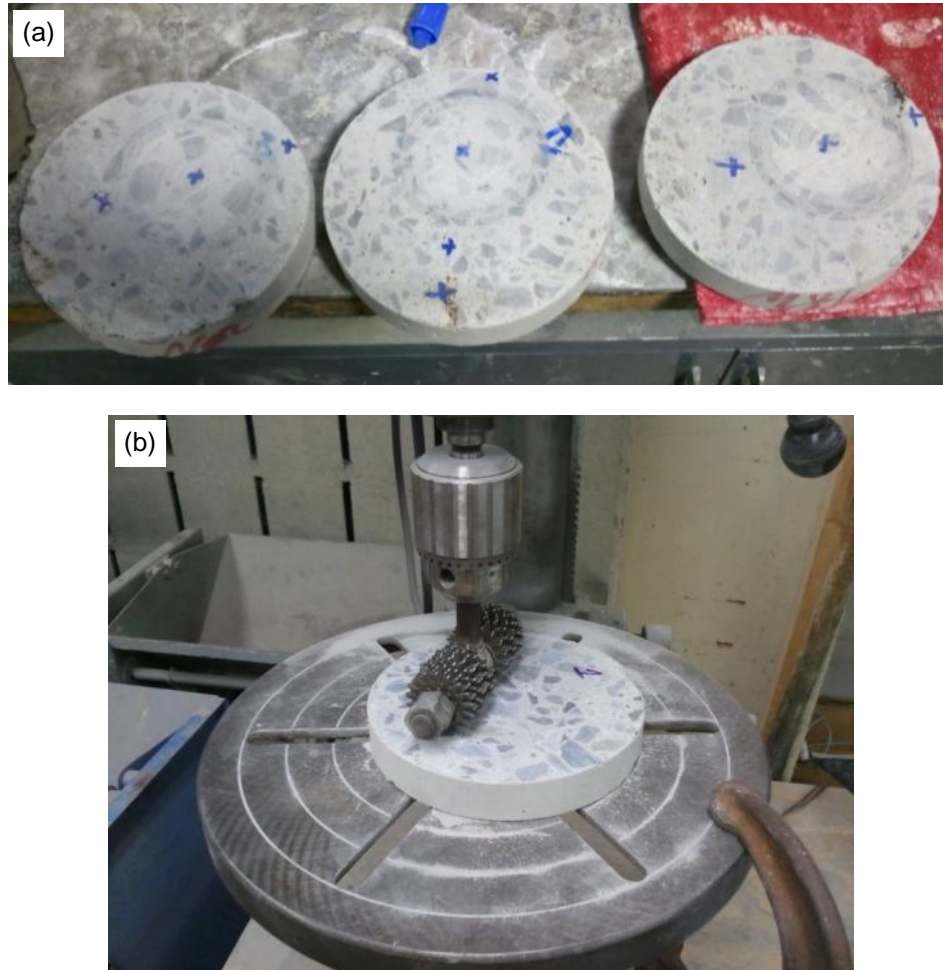

Figure 3-6: (a) Disk specimens used for abrasion resistance test; (b) ASTM C 944 test setup

3.3.6. Rapid chloride permeability test (ASTM C1202)

The ability of concrete to resist the penetration of aggressive elements (e.g., chloride ions) is key to the durability of reinforced concrete structures. External chloride ions (e.g., due to application of deicing salts or in marine environments) penetrate through concrete's cover layer and cause corrosion of the reinforcing steel bars (Figure 3-7) (Berke 1988). The steel corrosion products (rust) have a much larger volume, up to seven times the volume of the original steel. This volume expansion often causes large tensile stress development inside concrete and results in cracking and spalling of the concrete's cover, which exposes the corroding rebar (Berke et al. 1988).

Figure 3-7: Corrosion of steel reinforcing bars in concrete (Courtesy of Matco Services, Inc.).

To evaluate the resistance of glasscrete and natural sand concrete mixtures against penetration of chloride ion, the ASTM C1202 test was performed. Concrete cylinders (4 inches by 8 inches) were prepared and moist cured for 27 days. After curing, the cylinders were cut into 2-inch-thick disks obtained from the center of the cylinder. An epoxy resin was applied to the exterior of the disks to prevent lateral moisture loss. After the epoxy had set, the concrete disks were vacuum saturated by vacuum drying inside a desiccator for 3 hours, followed by filling the desiccator under vacuum with de-aired (boiled) water to submerge all specimens. The vacuum was allowed to run for an additional 1 hour. Next, the vacuum was shut off and the specimens were allowed to soak for an additional 18 hours. This procedure was intended to fully saturate the concrete pores with water. The specimens were subsequently removed and loaded into two half cells made of Plexiglas and sealed via silicone rubber (Figure 3-8). Each half cell had a reservoir that was filled with a solution of either 3.0% NaCl (at the negative half-cell) or 0.3 M NaOH (at the positive half-cell). After the silicone was allowed to dry overnight, the cells were filled with the solutions and the setup subjected to a 60 V DC voltage. The voltage forces the penetration of negative chloride ions into the concrete disk. As such, an electrical current flows into concrete, whose magnitude is a measure of rate of ion penetration. The voltage was applied for 6 hours with the electrical current and charge passed recorded automatically every 30 minutes. The results were adjusted based on the specimens' diameter according to ASTM C1202. The measurements were performed using RLC Instrument model 164A Test Set Power Supply. Two specimens from each mixture were tested at an age of 28 days.
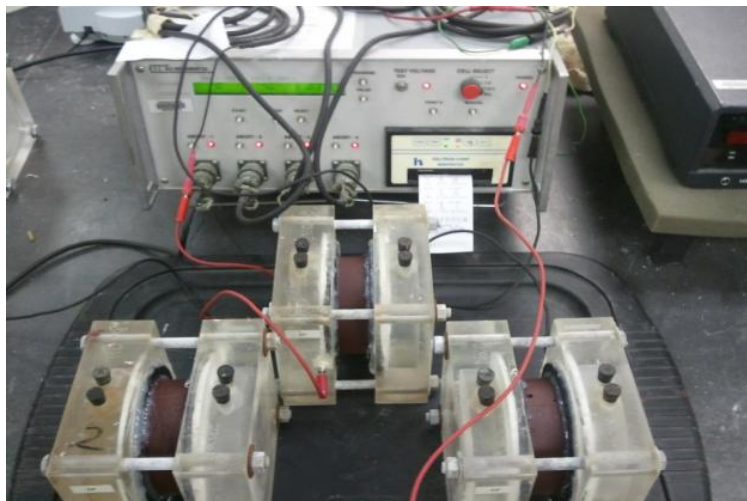

Figure 3-8: The rapid chloride permeability test setup (ASTM C1202)

Concrete with a higher w/cm has a greater volume of capillary porosity and thus allows for easier penetration of moisture and ions. ASTM C1202 provides a qualitative evaluation of concrete resistance to ion penetration using the magnitude of the electrical charge passed during the 6-hour test (Table 3-6). Large electrical current passing through high w/cm specimens can produce heat, thus increasing the temperature of the specimen (Stanish et al.1997). The increase in temperature serves as a positive feedback, leading to an artificial increase in the electrical current and the charge passed (Mindess et al. 2003). For this reason, during the test, the temperatures of the solutions were monitored periodically using a thermometer to ensure that they did not exceed 190 ^{0}F (90 ^{0}C). In addition, when the current exceeded 300 mA at the test's conclusion, the RCPT values were corrected to account for overheating. The correction was based on the current passed during the first 30 minutes of testing (Mindess 2003). The new ASTM C1760 test method allows for the use of electrical current passing during the first 1 minute of the test.

Table 3-6: Qualitative description of concrete chloride ion penetrability per ASTM C1202

Charge Passed (coulombs)	Chloride ion Penetrability
>4000	High
2000-4000	Moderate
1000-2000	Low
100-1000	Very Low
<100	Negligible

3.3.7. Water sorptivity test (ASTM C1585)

Moisture penetration inside concrete has a profound impact on its durability, as moisture may contain salts and other aggressive chemicals that attack concrete or the reinforcing steel. In addition, drying of moisture from concrete can cause shrinkage and cracking. One method used to quantify moisture transport in concrete is through sorptivity measurements. This test measures the rate of moisture absorption into an unsaturated concrete disk specimen. The typical test setup is shown in Figure 3-9, in which unsaturated concrete disks are exposed to water from their bottom surface. The sides are sealed with vinyl electrician's tape, while the top surface is covered by a plastic wrap to allow air to escape from the sample while preventing drying. Water is absorbed from the bottom surface into the concrete due to capillary forces. As such, the rate of water absorption (i.e., sorptivity) is significantly related to the magnitude of capillary forces, which is governed by the moisture content, pore size, and total porosity of concrete (Kelham 1988, Hall 1989). In addition, the absorption rate depends on the hydraulic permeability of concrete, which itself is a function of concrete porosity and pore size distribution (Martys and Ferraris 1997, Rajabipour et al. 2005, Castro et al. 2011). Overall, sorptivity is an easy test to perform; but the results are more difficult to properly interpret (Hall and Hoff 2002).

In this work, concrete was cast in 4-inch-by-8-inch cylinders and allowed to moist cure for twenty-eight (28) days. After curing, the cylinders were cut into 2-inch disks, allowing two disk specimens to be obtained for each mixture. The specimens were then conditioned by placing them in an environmental chamber at 50^{0}C and 80% RH for 3 days. Next, the specimens were individually packaged in sealable plastic containers and maintained at a temperature of 23 ^{0}C for 20 days to allow for the internal redistribution of moisture throughout the specimen (Castro et al. 2011). After proper conditioning, the exterior of the specimens were coated with vinyl electrician's tape to prevent air and moisture loss from the perimeter. Also, the top of the specimens were covered with a plastic sheet to allow only water to ingress through the bottom, while allowing the air to escape into the plastic sheet without allowing drying to occur from the top surface. In order to mitigate moisture ingress through the sides of the concrete, a

commercially available masonry waterproofing sealer was placed at the interface of the concrete and vinyl electrician's tape.
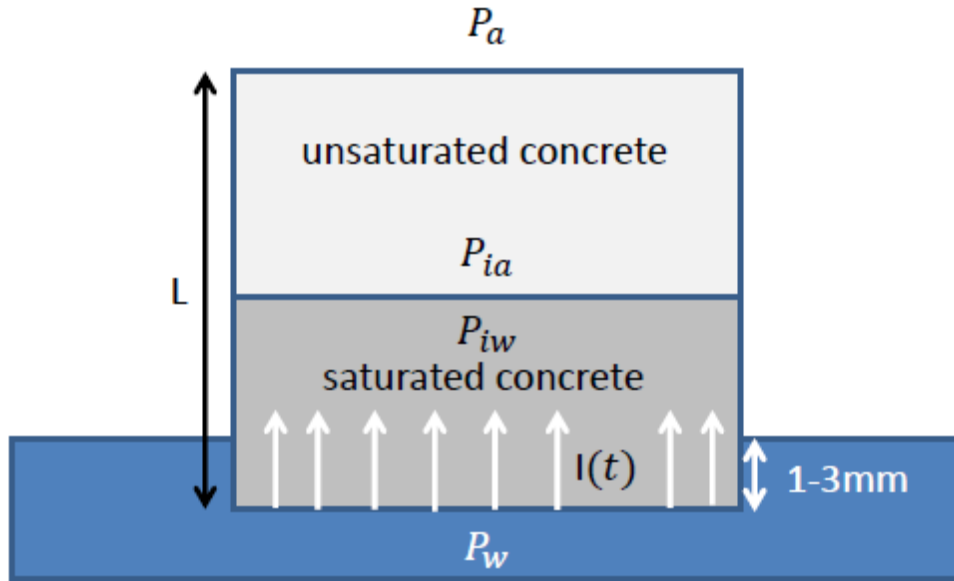

Figure 3-9: (Top) Schematics of a specimen's exposure to water during the sorptivity test; (bottom) Water bath setup in ASTM C1585

Mass recordings of the specimen were performed at predetermined intervals to determine the volumetric flux of absorbed water according to:

$$I = \frac{m_t}{a * d} \qquad (3\text{-}1)$$

where I (in or mm) is the volumetric absorption flux, m_t (lb or g) is the change in specimen's mass (i.e., mass of absorbed water) as a function of time (t), a (in^2 or mm^2) is the exposed cross sectional area of the specimen, and $d = 1$ mg/mm^3 = 62.4 lbs/ft^3 is the density of water. It can be shown that the volumetric absorption flux is linearly related to the square root of time (Kelham 1988):

$$I(t) = St^{0.5}$$

(3-2)

where S is termed sorptivity coefficient and has units of m/s$^{0.5}$ (or in/s$^{0.5}$).

3.4. Results

Tables 3-4 and 3-5 show the final mixture proportioning results for each concrete or mortar mixture after trial batch adjustments. Up to five trial batches were made for each mixture in order to match the target slump, air content, and compressive strengths. It can be seen in Table 3-4 that to achieve a similar compressive strength, the w/cm needs to be reduced for glasscrete mixtures. This is further discussed in section 3.4.3. The following summarizes the test results on fresh and hardened properties of glasscrete and natural sand concrete mixtures.

3.4.1. Fresh properties

A major task was finding the correct dosage of chemical admixtures (plasticizer and air-entrainer) to use in each mixture. The results are shown in Tables 3-7 and 3-8. Testing showed that for natural sand mixtures, the proper dosage of super-plasticizer was 0.007 to 0.074 fl.oz/lb of cementitious materials. The lower range was used for the 1.5-in slump and the higher range was for the 5.0-in slump mixtures. For glasscrete mixtures, the super-plasticizer dosage was in the range 0.007 to 0.038 fl.oz/lb of cementitious material. These values are well within and even below the dosage range recommended by the admixture manufacturer (0.02 to 0.15 fl.oz/lb). Regarding the air-entraining admixture, testing showed that for natural sand mixtures, the proper admixture dosage was 0.002 to 0.006 fl.oz/lb of cementitious material to achieve a target 3% air content. The lower range was used for the 1.5-in slump mixture and the higher range was for the 5.0-in slump mixtures. For glasscrete mixtures, the air entrainer dosage was found in the range 0.002 to 0.005 fl.oz/lb of cementitious material. These values are well within the range recommended by the admixture manufacturer (0.002 to 0.040 fl.oz/lb).

Table 3-7: Dosage of chemical admixture (fl.oz/lb cementitious material) used in each mixture

	N5,5.0"	G5,5.0"	N4,1.5"	G4,1.5"	N4,5.0"	G4,5.0"	N0.48,5.0"
w/cm	0.46	0.42	0.57	0.48	0.57	0.48	0.48
Plasticizer	0.058	0.038	0.007	0.007	0.074	0.037	0.061
Air-entrainer	0.005	0.005	0.002	0.002	0.006	0.005	0.005

Table 3-8: Dosage of chemical admixture (fl.oz/yd^3 of concrete) used in each mixture

	N5,5.0"	G5,5.0"	N4,1.5"	G4,1.5"	N4,5.0"	G4,5.0"	N0.48,5.0"
w/cm	0.46	0.42	0.57	0.48	0.57	0.48	0.48
Plasticizer	190	136	18	19	190	115	187
Air-entrainer	15	17	19	19	15	15	15

In order to achieve a similar slump of 5 inches, glasscrete required on average 30% to 40% less super-plasticizer than the natural sand concrete mixtures (Table 3-8). This is despite a lower w/cm that was necessary to achieve target compressive strengths in glasscrete mixtures. The super plasticizer demand was similar in 1.5-in slump mixtures, despite a considerably lower w/cm of the glasscrete. It should be noted that glasscrete mixtures with 5-in slump had slightly higher paste content that their natural sand

counterparts (Table 3-4), and this could improve workability to some degree. However, comparison of mixtures G4,5.0 and N0.48,5.0 show that even at the same paste content and w/cm, glasscrete required less plasticizer to achieve a 5-in slump (Table 3-8).

Previous studies have reported either an increase or a decrease in slump when fine glass aggregates were used as a natural sand substitution (Polley et al. 1998). Field workers noted that glasscrete mixtures demonstrated adequate workability and showed little problems with finishing (Polley et al. 1998). This study's results agree with Kou and Poon (2009) on improving workability and reducing super plasticizer demand when glass sand is used. The glass aggregate's smooth surfaces in comparison with rough surfaces of natural sand can result in lower surface area at similar particle sizes. The lower sand surface area can lead to better workability at similar paste content. Also, the smooth glass surface may produce a reduction in friction with the fresh cement paste and cause greater workability. At the same time, glass's angularity may reduce workability. This study observed that for glasscrete and natural sand concrete mixtures with slumps of 5 inches and similar w/cm or similar target 28-day strengths, glasscrete can achieve its designed slump with use of less plasticizer.

The fresh air content of concrete mixtures was measured according to ASTM C231. The target air content of 3.0% was attained via trial and error with multiple mixtures (Table 3-8). It can be seen that glasscrete and natural sand concrete mixtures with similar design slumps required approximately the same amount of air entrainer. Regardless of the mixture, air entrainer was necessary to attain the designed fresh air content.

3.4.2. Time of setting
The results of time of setting measurements of mortars according to ASTM C403 are reported in Table 3-9. Each data cell presented is the average of three measurements of initial or final set times performed on three duplicate specimens for each mixture. It can be seen that at similar design strengths, glasscrete mixtures show earlier initial and final set times when compared with their natural sand counterparts. This can be attributed to the lower w/cm of glasscrete mixtures resulting in faster setting, due to a lower initial porosity. However, at the same paste content and w/cm (G4,5.0 vs. G0.48,5.0), glasscrete still shows slightly faster setting; this could be attributed to a higher dosage of plasticizer in the natural sand mixture.

Table 3-9: ASTM C 403 time of setting of mortars (hours: minutes)

	N5,5.0"	G5,5.0"	N4,1.5"	G4,1.5"	N4,5.0"	G4,5.0"	N0.48,5.0"
w/cm	0.46	0.42	0.57	0.48	0.57	0.48	0.48
Paste Content	53.8%	55.9%	47.7%	46.0%	48.1%	51.5%	51.5%
Initial Set	4:40	4:25	6:30	5:05	5:50	5:10	5:45
Final Set	6:20	5:45	8:25	6:40	7:30	6:40	7:10

3.4.3. Compressive strength
Using trial batches, mixture proportions were adjusted using 7-day compressive strengths. After finalizing the proportions (e.g., w/cm), larger mixtures were batched that allowed the testing of the concrete's compressive strength at 1, 3, 7, 28, and 90 days. For each mixture and at each age, three duplicate specimens were tested. Table 3-10 provides strength results for the various mixtures. Figures 3-10 through 3-13 are also provided to show the strength gain over time for each mixture. The coefficient of variation of strength measurements are offered in Table 3-11. ASTM C39 suggests that the coefficient of variation shall be less that 3.2% for the single lab, single operator measurements. These precision values are suggested for 4-inch-by-8-inch cylinders with compressive strengths between 2,500 and 4,700 psi. In this study, most of the strength results comply with the precision statement of ASTM. However, some values fall outside the suggested precision values, and this may be a function of using unbounded caps instead of bounded caps (the load frame is calibrated annually). A comparison between glass sand

and natural sand mixtures shows that glasscrete mixtures do not increase the variability of concrete strength measurements.

Table 3-10: Age-dependent compressive strength of glasscrete and natural sand concrete mixtures (psi)

	N5,5.0"	G5,5.0"	N4,1.5"	G4,1.5"	N4,5.0"	G4,5.0"	N0.48,5.0"
w/cm	0.46	0.42	0.57	0.48	0.57	0.48	0.48
Paste content	32.9%	34.2%	29.2%	28.1%	29.5%	31.5%	31.5%
1-day	2190	2700	1410	2380	1420	1900	2010
3-day	3520	3410	2250	2900	2250	2640	3380
7-day	4290	4060	3250	3130	2950	2950	3970
28-day	5420	5060	4040	4240	4200	4070	4750
90-day	6440	6070	4480	5290	4820	5160	5610

Table 3-11: Coefficient of variation of compressive strength measurements

	N5,5.0"	G5,5.0"	N4,1.5"	G4,1.5"	N4,5.0"	G4,5.0"	N0.48,5.0"
1-day	4.3	1.7	0.3	4.2	4.8	1.2	9.0
3-day	1.7	4.1	8.4	4.5	1.2	2.8	1.3
7-day	3.3	1.0	4.2	2.1	3.2	4.0	4.1
28-day	1.3	3.2	4.5	4.3	1.5	4.4	3.0
90-day	4.8	2.9	5.6	3.7	0.9	3.2	1.7
Avg.	3.1	2.6	4.6	3.8	2.3	3.1	3.8

It is clearly demonstrated in Table 3-10 that glasscrete systems need a reduction in w/cm to achieve a similar design 28-day compressive strength. This is better represented in Figures 3-14 and 3-15, which show the correlation between the w/cm and the 7-day or 28-day compressive strength of both types of concrete. For example, based on the results in Figure 3-15, to achieve a 28-day strength of 4,500 psi, the natural sand concrete could be designed with w/cm = 0.53; however, the same target strength can be achieved in glasscrete only when the w/cm is decreased to 0.45. The lower strength of glasscrete mixtures is potentially due to weaker paste-aggregate bonding when glass sand is used. This hypothesis requires further investigation. Irrespective of the exact cause of strength reduction, diagrams such as those presented in Figures 3-14 and 3-15 can serve as valuable design tools for material designers when proportioning concrete mixtures containing glass sand.
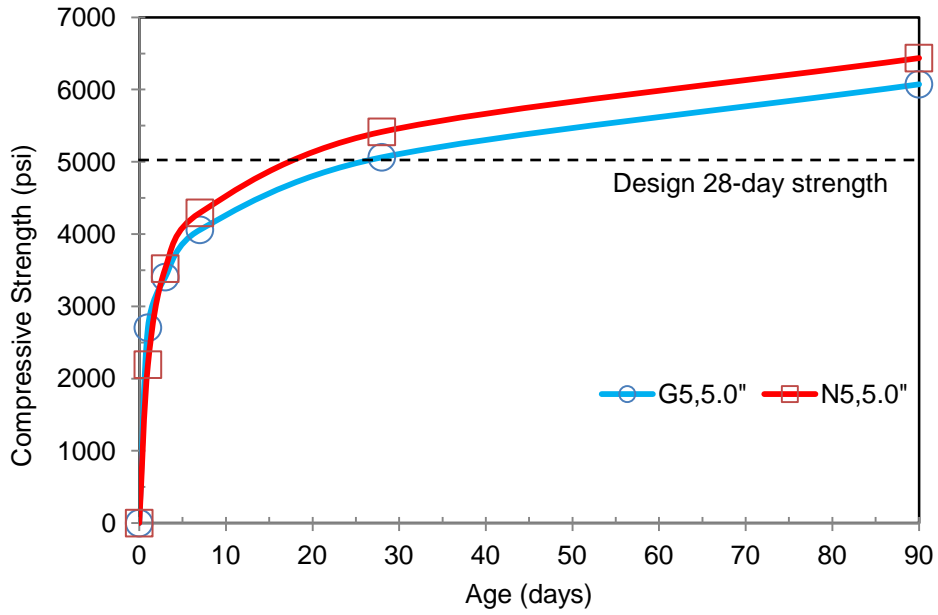
Figure 3-10: Compressive strength gain for G5,5.0-inch and N5,5.0-inch mixtures
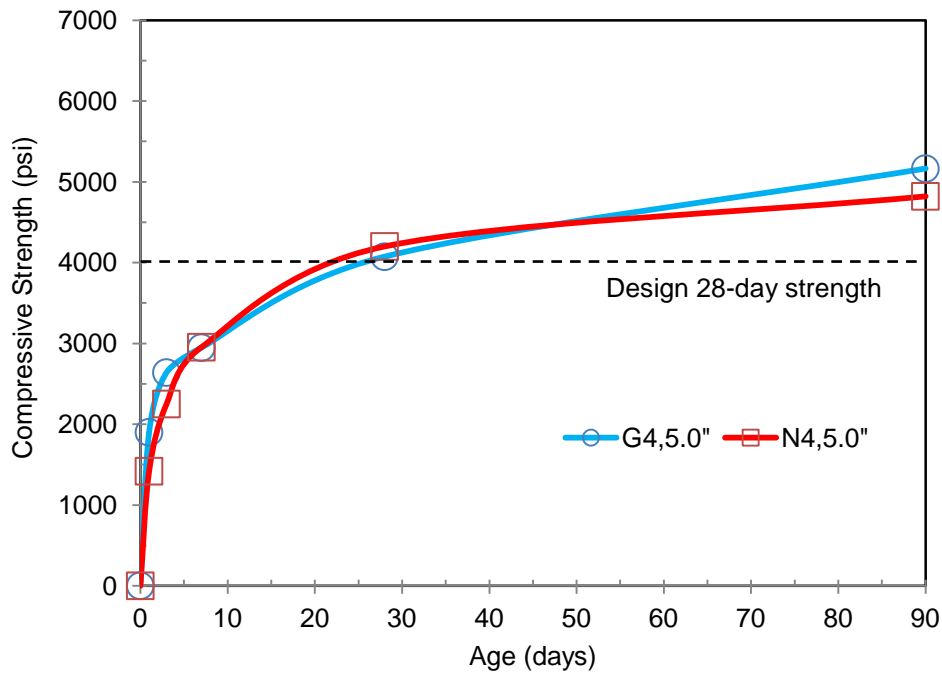

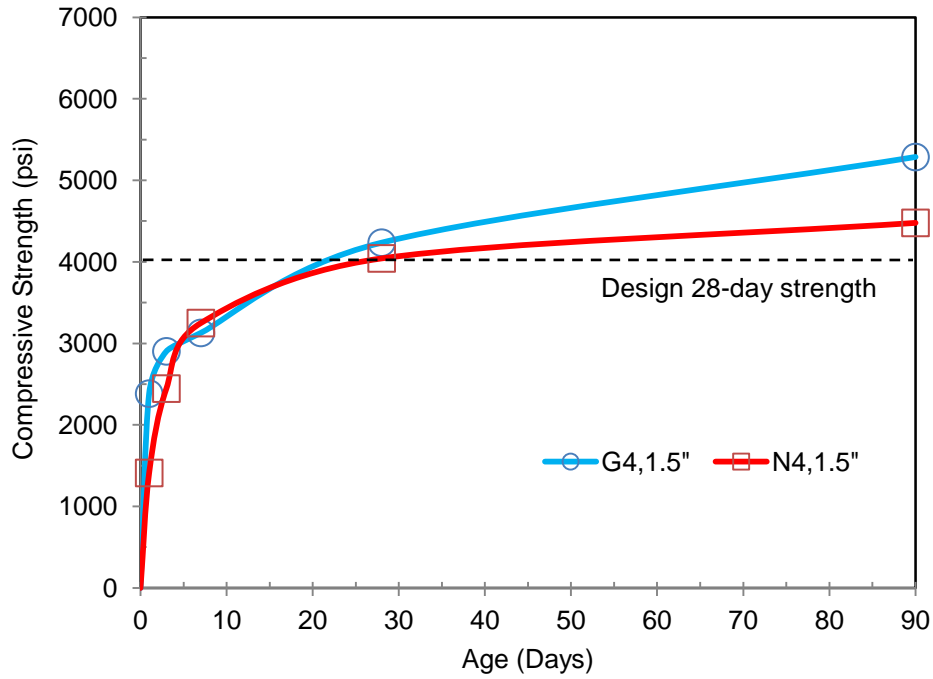Figure 3-11: Compressive strength gain for G4,5.0-inch and N4,5.0-inch mixtures

Figure 3-12: Compressive strength gain for G4,1.5-inch and N4,1.5-inch mixtures
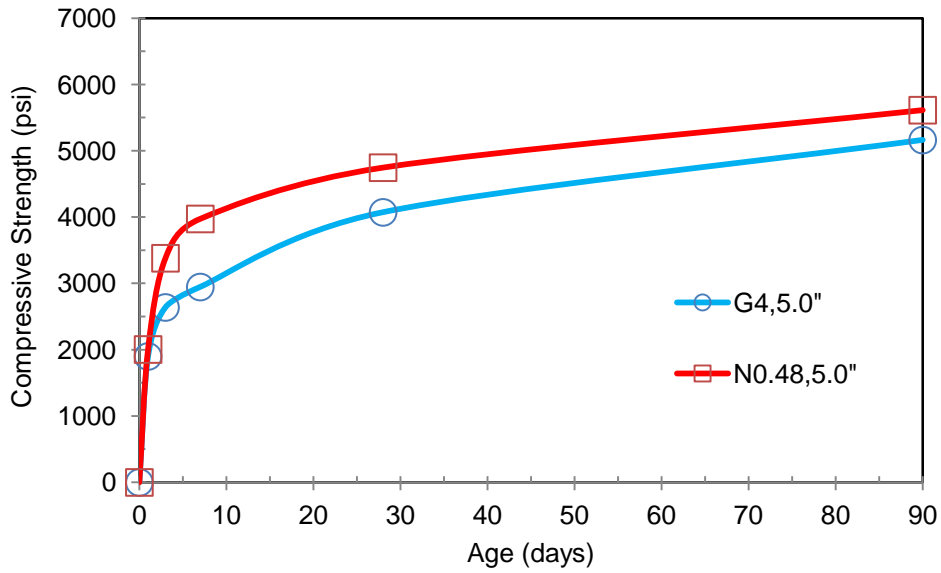

Figure 3-13: Compressive strength gain for G4,5.0-inch and N0.48,5.0-inch mixtures
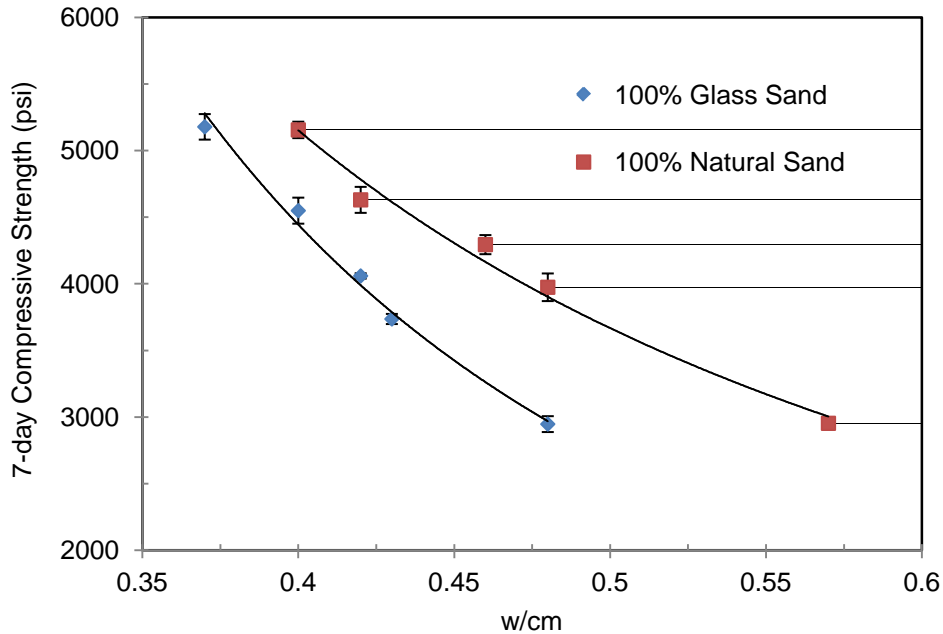
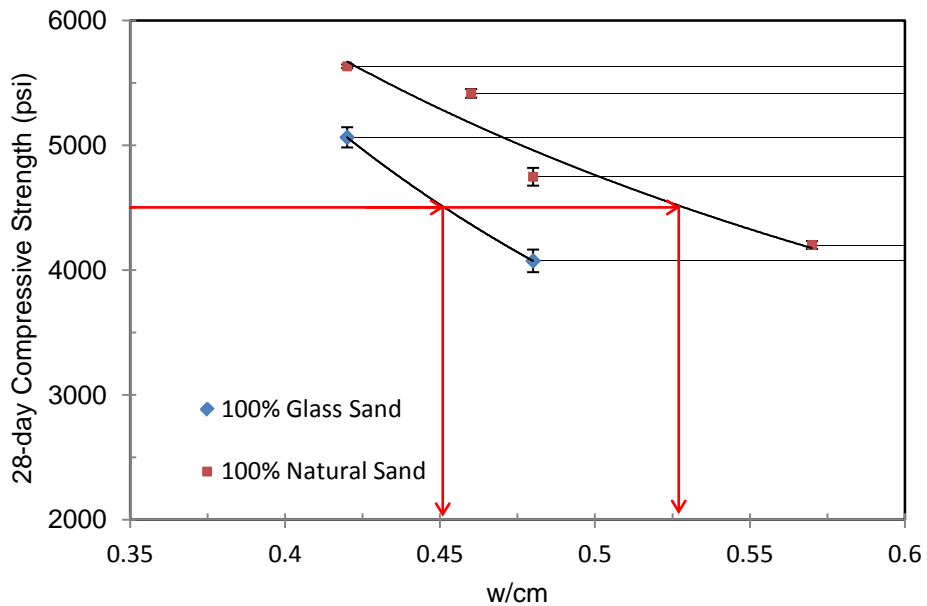Figure 3-14: Correlation between w/cm and 7-day compressive strength

Figure 3-15: Correlation between w/cm and 28-day compressive strength

3.4.5. Coefficient of thermal expansion (COTE)

The COTE measurement results for saturated mortars are provided in Table 3-12. It is observed that glasscrete mortars generally show a smaller COTE than natural sand mortars. Given that glasscrete mortars have a slightly higher cement paste content (which has higher COTE than aggregates, Table 3-13), such decrease in COTE of mortars could be due to (a) a lower COTE of glass sand in comparison with natural sand, and/or (b) a lower w/cm of glasscrete mortar. Table 3-13 shows typical COTE values for common rocks, soda-lime glass, as well as cement paste. It can be noted that with the exception of

basalt, most common aggregates that are contained in natural sand can have COTE that exceeds that of soda-lime glass. This is likely the reason that mortar G4,5.0 shows a slightly smaller COTE than mortar N0.48,5.0 despite their similar w/cm and paste content. It should also be noted that COTE was measured at the saturated state to prevent variation due to changing moisture contents of mortars.

Table 3-12: Coefficient of thermal expansion of saturated natural sand and glass sand mortars

Mixture	w/cm	Paste Content	Saturated COTE $(10^{-6}/^0F)$
N5,5.0"	0.46	53.8%	5.79
G5,5.0"	0.42	55.9%	4.13
N4,1.5"	0.57	47.7%	5.79
G4,1.5"	0.48	46.0%	5.43
N4,5.0"	0.57	48.1%	4.99
G4,5.0"	0.48	51.5%	5.20
N0.48,5.0"	0.48	51.5%	5.48

Table 3-13: Coefficient of thermal expansion of common rocks, glass, concrete, and cement paste (Neville 1995; Mindess et al. 2003)

Material	COTE $(10^{-6}/^0F)$
Basalt, Gabbro	2.4-4.4
Granite, Rhyolite	2.8-6.1
Limestone	2.2-6.7
Sandstone	4.4-6.7
Quartzite	6.1-7.2
Soda-Lime Glass	4.0-5.0
Concrete	4.1-7.3
Steel	11.0-12.0
Cement paste	10.3

3.4.6.   Abrasion resistance
The ASTM C944 abrasion results are provided in Table 3-14. Glasscrete mixtures typically show a better abrasion resistance than natural sand concrete at the same design strength. However, this is likely due to the lower w/cm of glasscrete, which is known to create a stronger and more abrasion-resistant cement paste matrix (Neville 1995, Mindess et al. 2003). At the same w/cm, glasscrete shows considerably lower abrasion resistance, which is likely due to a weaker aggregate-paste bonding.

Table 3-14: Average mass loss of three duplicate specimens after the 6-minute abrasion test

	N5,5.0"	G5,5.0"	N4,1.5"	G4,1.5"	N4,5.0"	G4,5.0"	N0.48,5.0"
w/cm	0.46	0.42	0.57	0.48	0.57	0.48	0.48
Mass loss (g)	0.90	0.77	0.93	0.80	0.90	0.97	0.60

3.4.7. Rapid chloride permeability

The RCPT results (Table 3-15) demonstrate that glasscrete mixtures have a greater resistance to chloride ion penetration than natural sand concrete at both similar compressive strengths and similar w/cm. The improved resistance at similar design strengths was anticipated due to lower w/cm (and paste porosity) of glasscrete mixtures. However, a better RCPT at similar w/cm suggests that glasscretes are less ion-penetrable than natural sand mixtures and this is likely due to the absence of porosity in glass aggregates, which blocks the penetration path of ions. These results suggest that properly produced and constructed glasscrete can have better durability than conventional concrete due to an improved resistance against mass transport. This observation is also in agreement with the water sorptivity measurements presented in the following section.

Table 3-15: RCPT results (Coulombs), **bold** were overheated

	N5,5.0"	G5,5.0"	**N4,1.5"**	G4,1.5"	**N4,5.0"**	G4,5.0"	N0.48,5.0"
w/cm	0.46	0.42	0.57	0.48	0.57	0.48	0.48
Charge passed (Coulombs)	3220	2320	5040	1920	4480	2540	3080
Ion penetration resistivity	Moderate	Moderate	High	Moderate to Low	High	Moderate	Moderate

3.4.8. Water sorptivity

An example of the water sorptivity measurements is provided in Figure 3-16 for the mixture G5,5.0. The graph shows the volumetric flux of the absorbed water (I) as a function of the square root of time. Based on the slope of the tangent to data points, initial and secondary sorptivity coefficients can be calculated according to ASTM C1585. Similar measurements were performed on specimens from other mixtures. The sorptivity coefficients were determined by testing two duplicate specimens per mixture and the results are reported in Table 3-16. The sorptivity of glasscrete is consistently and significantly smaller than that for natural sand concrete when the two have the same compressive strength. As with the RCPT measurements, this was anticipated since glasscrete has a lower w/cm to achieve similar target strength. When the two concretes are compared on the same w/cm basis, glasscrete still shows consistently better sorptivity coefficients, which is likely due to the absence of aggregate porosity for glass fine aggregates.
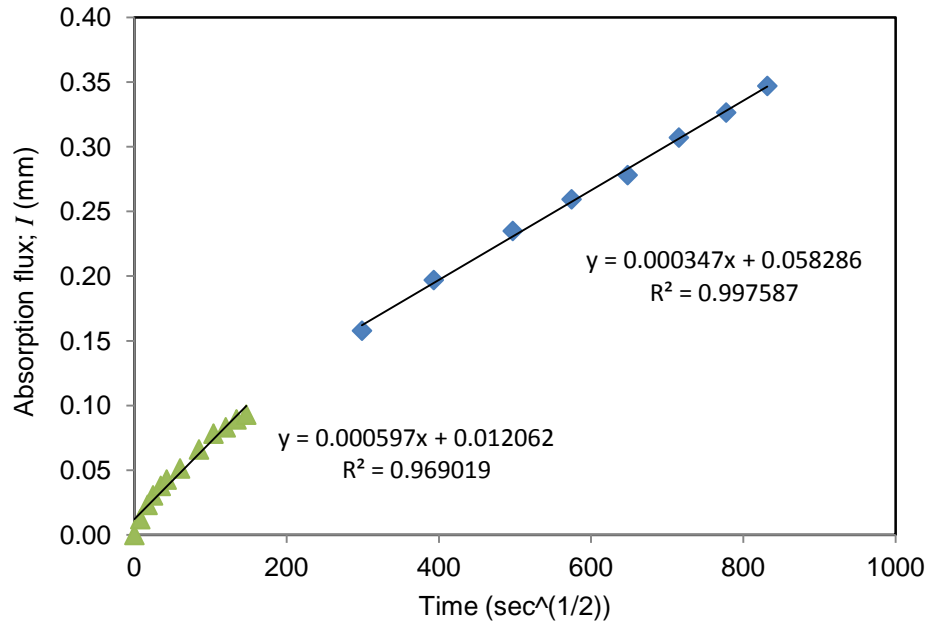
Figure 3-16: Results of sorptivity test for the mixture G5,5.0

Table 3-16: Sorptivity coefficients (10^{-4}mm/sec$^{0.5}$)

	N5,5.0"	G5,5.0"	N4,1.5"	G4,1.5"	N4,5.0"	G4,5.0"	N0.48,5.0"
w/cm	0.46	0.42	0.57	0.48	0.57	0.48	0.48
Initial Sorptivity	13.3	6.74	34.6	9.23	37.4	10.0	15.8
Final Sorptivity	11.7	5.46	28.1	9.25	26.8	6.41	13.8

3.5.   Conclusions

The focus of this chapter was proportioning and testing glasscrete mixtures (i.e., concrete mixtures containing recycled glass as 100% replacement of natural fine aggregates. A total of seven concrete mixtures were prepared and tested, including three glasscretes and four natural sand concretes. The fresh and hardened properties of the two types of concretes were compared on the basis of similar target 28-day compressive strength or similar w/cm and cement paste content. Based on the measurements, the following conclusions can be drawn:

- Glasscrete mixtures have a lower compressive strength than natural sand concrete at the same w/cm. As such, to achieve a target strength, a lower w/cm must be used when designing glasscrete mixtures. Design graphs were developed in this work that relate the w/cm of glasscrete to the 7-day and 28-day compressive strength of the material.

- Glasscrete mixtures require less plasticizer to achieve a target slump. This may be due to the smooth surfaces of glass particles that create a smaller surface area (for a given aggregate size) and also reduce friction in a plastic concrete.

- Glasscrete sets slightly faster than conventional concrete. This is especially true for similar design strength, which requires a lower w/cm for glasscrete.

- Glasscrete tends to show a lower coefficient of thermal expansion than conventional concrete. This is likely due to lower COTE of glass in comparison with most natural aggregates.

- At similar w/cm, glasscrete shows an inferior abrasion resistance than natural sand concrete. This is likely the result of weaker glass aggregate-paste bonding.

- Glasscrete shows a consistently better resistance against penetration of moisture and ions. This is based on the results of rapid chloride permeability measurements as well as water sorptivity measurements. This conclusion is valid for comparison on the basis of similar compressive strength as well as on the basis of similar w/cm and is likely the result of absence of porosity in glass aggregates, which blocks the pathways for penetration of moisture and ions.

References
- ACI 211.1-91, Standard Practice for Selecting Proportions for Normal, Heavyweight, and Mass Concrete, Reapproved 2009, American Concrete Institute, Farmington Hills, Michigan, USA
- ACI 231R-10: Report on Early-Age Cracking: Causes, Measurement, and Mitigation, American Concrete Institute, Farmington Hills, Michigan, USA
- ASTM C 33 – 07, Standard Specification for Concrete Aggregates, 2007, American Society for Testing and Materials, West Conshohocken, Pennsylvania, USA
- ASTM C 39/C 39M – 05, Standard Test Method for Compressive Strength of Cylindrical Concrete Specimens, 2005, American Society for Testing and Materials, West Conshohocken, Pennsylvania, USA
- ASTM C 125 – 07, Standard Terminology Relating to Concrete and Concrete Aggregates, 2007, American Society for Testing and Materials, West Conshohocken, Pennsylvania, USA
- ASTM C 143/C 143M – 05a, Standard Test Method for Slump of Hydraulic-Cement Concrete, 2005, American Society for Testing and Materials, West Conshohocken, Pennsylvania, USA
- ASTM C150/C150M-11, Standard Specification for Portland Cement, 2011, American Society for Testing and Materials, West Conshohocken, Pennsylvania, USA
- ASTM C 231 – 08, Standard Test Method for Air Content of Freshly Mixed Concrete by the Pressure Method, 2008, American Society for Testing and Materials, West Conshohocken, Pennsylvania, USA
- ASTM C 403/C 403M – 06, Standard Test Method for Time of Setting of Concrete Mixtures by Penetration Resistance, 2006, American Society for Testing and Materials, West Conshohocken, Pennsylvania, USA
- ASTM C 531 – 00, Standard Test Method for Linear Shrinkage and Coefficient of Thermal Expansion of Chemical-Resistant Mortars, Grouts, Monolithic Surfacings, and Polymer Concretes, reapproved 2005, American Society for Testing and Materials, West Conshohocken, Pennsylvania, USA
- ASTM C618-08a, Standard Specification for Coal Fly Ash and Raw or Calcined Natural Pozzolan for Use in Concrete, 2008, American Society for Testing and Materials, West Conshohocken, Pennsylvania, USA
- ASTM C 944/C 944M – 99, Standard Test Method for Abrasion Resistance of Concrete or Mortar Surfaces by the Rotating-Cutter Method, reapproved 2005, American Society for Testing and Materials, West Conshohocken, Pennsylvania, USA
- ASTM C 1202 – 07, Standard Test Method for Electrical Indication of Concrete's Ability to Resist Chloride Ion Penetration, 2007, American Society for Testing and Materials, West Conshohocken, Pennsylvania, USA
- ASTM C 1585 – 04, Standard Test Method for Measurement of Rate of Absorption of Water by Hydraulic-Cement Concretes, 2004, American Society for Testing and Materials, West Conshohocken, Pennsylvania, USA
- ASTM C 1760 – 12, Standard Test Method for Bulk Electrical Conductivity of Hardened Concrete, 2012, American Society for Testing and Materials, West Conshohocken, Pennsylvania, USA
- Z.P. Bazant, 'Delayed thermal dilations of cement paste and concrete due to mass transport', Nuclear Engineering and Design, 14 (1970) 308-318

- N.S. Berke, D.W. Pfeifer, T.G. Weil, 'Protection against chloride-induced corrosion', Concrete International, 10(12) (1988) 45-55
- J. Castro, D. Bentz, J. Weiss, 'Effect of sample conditioning on the water absorption of concrete', Cement and Concrete Composites, (33) (2011) 805-813
- J.H. Emanuel, J.L. Hulsey, 'Prediction of the thermal coefficient of expansion of concrete', ACI Journal, 74(4) (1977) 149-155
- Z. Grasley, 'Internal relative humidity, drying stress gradients, and hygrothermal dilation of concrete', M.S. Thesis, University of Illinois at Urbana-Champaign, Champaign, IL, 2003
- C. Hall, 'Water sorptivity of mortars and concretes: A review', Magazine of Concrete Research, 41 (1989) 51-61
- C. Hall, W.D. Hoff, Water Transport in Brick Stone and Concrete, Spon Press, New York, 2002
- S. Kelham, 'A water absorption test for concrete', Magazine of Concrete Research, 40(143) (1988) 106-110
- S.H. Kosmatka, M.L. Wilson, Design and Control of Concrete Mixtures, 15th Ed., 2011, Portland Cement Association, Skokie, Illinois, USA
- S.C. Kou, C.S. Poon, 'Properties of self-compacting concrete prepared with recycled glass aggregate', Cement and Concrete Composites 31 (2009) 107-113
- S. Mindess, J.F. Young, D. Darwin, Concrete, 2nd Ed., 2003, Pearson Education, Upper Saddle River, New Jersey, USA
- A.M. Neville, Properties of Concrete, 4th Ed., 1995, Pearson Education, Harlow, Essex, England
- C. Polley, S.M. Cramer, R.V. de la Cruz, Potential for using waste glass in portland cement concrete, ASCE Journal of Materials in Civil Engineering, 10 (4) (1998) 210-219
- S. Popovics, Analysis of the Concrete Strength Versus Water-Cement Ratio Relationship, ACI Materials Journal, 87(5) (1990) 517-529
- F. Rajabipour, J. Weiss, J.D. Shane, T.O. Mason, S.P. Shah, 'Procedure to interpret electrical conductivity measurements in cover concrete during rewetting', ASCE Journal of Materials in Civil Engineering, 17(5) (2005) 586-594
- F. Rajabipour, G. Fischer, P. Sigurdardottir, S. Goodnight, A. Leake, E. Smith, Recycling and utilizing waste glass as concrete aggregate, Proceedings of TRB Annual Meeting, 2009, CD-Rom Paper# 09-2195, Transportation Research Board, Washington, DC, USA
- E. J. Sellevold, Ø. Bjøntegaard, 'Coefficient of thermal expansion of cement paste and concrete: Mechanisms of moisture interaction', Materials and Structures, 39 (9) (2006) 809-815
- K.D. Stanish, R.D. Hooton, R.D., M.D.A. Thomas, 'Testing the chloride penetration resistance of concrete: A literature review', FHWA contract DTFH61-97-00022, Department of Civil Engineering, University of Toronto, Ontario, Canada, 1997
- T.R. West, Geology Applied to Engineering, Prentice Hall, 1994, 560 pp.
- C.G. Zoldners, Thermal properties of concrete under sustained elevated temperatures, ACI SP-25, (1971) pp. 1-32

CHAPTER 4:
SUMMARY AND CONCLUSIONS

The environmental impact of Portland cement concrete production has motivated researchers and the construction industry to evaluate alternative technologies for incorporating recycled cementing materials and recycled aggregates in concrete. One such technology is based on using pulverized glass as sand or pozzolan. Currently in the U.S., more than 600,000 tons/year of recycled glass bottles are stockpiled due to prohibitive shipping costs from recycling locations to glass melting factories. This project has proposed the use of this waste material along with fly ash (another industrial byproduct with landfill rate of 42.4 million tons/year) in developing durable and environmentally positive concretes that can be used for various transportation applications.

The main challenge in producing durable glass-based concretes is the deleterious alkali-silica reaction (ASR) between glass particles and the cement paste matrix. The amorphous silicate structure of glass is attacked by hydroxyl (OH^-) ions in concrete's pore solution. As such, glass aggregates gradually dissolve and are converted to a highly hygroscopic silica gel that absorbs water, swells, and cracks concrete. In this project, fly ash was used to mitigate potential ASR deteriorations that could otherwise occur due to use of siliceous glass aggregates. Prior research on natural siliceous aggregates (e.g., opal) has shown that ASTM C618 fly ash can be effective in controlling ASR expansions; however, it is not clear how fly ash mitigates ASR. To optimize the use of fly ash and minimize the potential negative impacts on concrete's early-age strength, it is important to determine exactly how fly ash prevents ASR and what ash properties (e.g., composition, fineness, glass content) determine its effectiveness. Furthermore, it is important to evaluate the properties of concrete containing glass fine aggregates and fly ash to ensure that such concretes can be produced with desired strength, workability, and durability.

As such, this project aimed at two major technical objectives:
1- Understanding the mechanism by which fly ash mitigates ASR, and identifying factors that most significantly determine fly ash effectiveness against ASR;
2- Preparation and evaluation of concrete mixture that includes glass fine aggregates and fly ash to ensure desirable early-age and long-term performance.

Accordingly, the project included two main tasks that were presented in Chapters 2 and 3 of this report. In Task 1 (Chapter 2), a quantitative evaluation of six potential mechanisms by which fly ash could control ASR in concrete materials containing glass fine aggregates was performed. Six fly ashes of different compositions (including four class F and two class C fly ashes) were studied to evaluate the effect of fly ash properties on its effectiveness against ASR. A variety of analytical tools were used to study the material's microstructure, its mechanical and transport properties, pore solution composition, aggregate dissolution rate, and ASR gel formation and composition. The results of this task suggest that fly ash can effectively mitigate ASR per ASTM C1567 (accelerated mortar bar) test through the following mechanisms:

- Fly ash reduces the alkalinity ($[OH^-]$) of pore solution by significantly reducing the ion diffusion coefficient of mortars. A diffusivity reduction by a factor of 4 to 7 was recorded, as early as 48 hours after casting, when sufficient dosage of fly ash replaced Portland cement. As such, the external NaOH penetrates slower into fly ash mortars, resulting in a lower pore fluid alkalinity and significantly slower ASR.

- Fly ash reduces the alkalinity ($[OH^-]$) of pore solution through alkali binding. Fly ash reduces the calcium to silica ratio (C/S) of C-S-H gel, which in turn improves its alkali binding capacity. In addition, more C-S-H is produced by pozzolanic reactions. As such, a considerable fraction of the penetrated NaOH is removed from the pore solution. The results of a simple numerical model suggested that the contribution of transport reduction is more significant than the effect of improved alkali binding.

- Fly ash increases the tensile strength of mortars and prevents or delays the onset of cracking. This also prevents an accelerated transport of NaOH through cracks to the interior of mortar specimens.

- Fly ash can reduce the dissolution rate of siliceous aggregates even when the pH of pore solution is maintained constant (e.g., near the perimeter of mortar prisms that are exposed to an external NaOH bath). Fly ash provides a large silicate surface area that is accessible to the corrosive OH^- ions. As such, the concentration of OH^- per unit surface area of silicate is markedly reduced. In other words, for a unit volume of pore solution at a given pH, a significant fraction of hydroxyl ions are involved in dissolving fly ash instead of attacking the reactive aggregates.

Task 2 (Chapter 3) used the findings of Task 1 in mixture proportioning of concrete mixtures containing recycled glass sand. Most importantly, the effects of using glass sand on concrete strength and other fresh and hardened properties were evaluated and proportioning charts were developed that relate concrete's w/cm to its strength. A total of seven concrete mixtures were prepared and tested, including three glasscretes and four natural sand concretes. The fresh and hardened properties of the two types of concretes were compared on the basis of similar target 28-day compressive strength or similar w/cm and cement paste content. Based on the measurements, the following conclusions can be drawn:

- Glasscrete mixtures have a lower compressive strength than natural sand concrete at the same w/cm. As such, to achieve a target strength, a lower w/cm must be used when designing glasscrete mixtures. Design graphs were developed in this work that relate the w/cm of glasscrete to the 7-day and 28-day compressive strengths of the material.

- Glasscrete mixtures require less plasticizer to achieve a target slump. This may be due to the smooth surfaces of glass particles that create a smaller surface area (for a given aggregate size) and also reduce friction in a plastic concrete.

- Glasscrete sets slightly faster than conventional concrete. This is especially true for similar design strengths, which require a lower w/cm for glasscrete.

- Glasscrete tends to show a lower coefficient of thermal expansion than conventional concrete. This is likely due to lower COTE of glass in comparison with most natural aggregates.

- At similar w/cm, glasscrete shows an inferior abrasion resistance than natural sand concrete. This is likely the result of weaker glass aggregate-paste bonding.

- Glasscrete shows a consistently better resistance against penetration of moisture and ions. This is based on the results of rapid chloride permeability measurements as well as water sorptivity measurements. This conclusion is valid for comparison on the basis of similar compressive strength as well as on the basis of similar w/cm and is likely the result of the absence of porosity in glass aggregates, which blocks the pathways for penetration of moisture and ions.